2-6-2024

Deep Structure of Siletzia in the Puget Lowland: Imaging an Obducted Plateau and Accretionary Thrust Belt With Potential Fields

Megan L. Anderson
Washington Geological Survey

Richard J. Blakely
U.S. Geological Survey

Ray E. Wells
Portland State University, rwells@pdx.edu

Joe D. Dragovich
Dragovich Geo-Consulting

Citation Details

Anderson, M. L., Blakely, R. J., Wells, R. E., & Dragovich, J. D. (2024). Deep structure of Siletzia in the Puget Lowland: Imaging an obducted plateau and accretionary thrust belt with potential fields. Tectonics, 43(2), e2022TC007720.

Deep Structure of Siletzia in the Puget Lowland: Imaging an obducted plateau and accretionary thrust belt with potential fields

Megan Anderson[1], Richard Blakely[2], Ray E. Wells[2], and Joe D. Dragovich[3]

[1]Washington Geological Survey
[2]United States Geological Survey
[3]Dragovich Geo-Consulting

December 17, 2022

Abstract

Detailed understanding of crustal components and tectonic history of forearcs is important, due to their geological complexity and high seismic hazard. The principal component of the Cascadia forearc is Siletzia, a composite basaltic terrane of oceanic origin. Much is known about the lithology and age of the province. However, glacial sediments blanketing the Puget lowland obscure its lateral extent and internal structure, hindering our ability to fully understand its tectonic history and its influence on modern deformation. In this study, we apply map-view interpretation and two-dimensional modeling of aeromagnetic and gravity data to the magnetically stratified Siletzia terrane revealing its internal structure and characterizing its eastern boundary. These analyses suggest the contact between Siletzia (Crescent Formation) and the Eocene accretionary prism trends northward under Lake Washington. North of Seattle, this boundary dips east where it crosses the Kingston arch, while south of Seattle the contact dips west where it crosses the Seattle uplift. This westward dip is opposite of the dip of the Eocene subduction interface, implying obduction of Siletzia upper crust at this location. Elongate pairs of high and low magnetic anomalies over the Seattle uplift suggest imbrication of steeply-dipping, deeply-rooted slices of Crescent Formation within Siletzia. We hypothesize these features result from duplication of Crescent Formation in an accretionary fold-thrust belt during the Eocene. The active Seattle fault divides this Eocene fold-thrust belt into two zones with different structural trends and opposite frontal ramp dips, suggesting the Seattle fault may have originated as a tear fault during accretion.

Hosted file

`952252_0_art_file_10540327_rmy73r.docx` available at https://authorea.com/users/531670/articles/613614-deep-structure-of-siletzia-in-the-puget-lowland-imaging-an-obducted-plateau-and-accretionary-thrust-belt-with-potential-fields

Hosted file

`952252_0_supp_10540328_rmy73r.docx` available at https://authorea.com/users/531670/articles/613614-deep-structure-of-siletzia-in-the-puget-lowland-imaging-an-obducted-plateau-and-accretionary-thrust-belt-with-potential-fields

Hosted file

`952252_0_supp_10540329_rmy73r.docx` available at https://authorea.com/users/531670/articles/613614-deep-structure-of-siletzia-in-the-puget-lowland-imaging-an-obducted-plateau-and-accretionary-thrust-belt-with-potential-fields

Hosted file

952252_0_supp_10540330_rmy73r.docx available at https://authorea.com/users/531670/articles/613614-deep-structure-of-siletzia-in-the-puget-lowland-imaging-an-obducted-plateau-and-accretionary-thrust-belt-with-potential-fields

Deep Structure of Siletzia in the Puget Lowland: Imaging an obducted plateau and accretionary thrust belt with potential fields

M. L. Anderson[1], R. J. Blakely[2], R. E. Wells[2], and J. D. Dragovich[3]

[1]Washington Geological Survey, 1111 Washington St. SE, MS 47007, Olympia, WA, 98504. [2]U.S. Geological Survey, East Hall, Portland State University, 632 Hall Street, Portland, Oregon, 97201. [3]Dragovich Geo-Consulting, 3050 Carpenter Hills Loop Southeast, Lacey, Washington, 98503.

Corresponding author: Megan Anderson (megan.anderson@dnr.wa.gov)

Key Points:

- Includes map interpretation and models of the upper crust utilizing constraints from gravity, aeromagnetics, seismology and geology.
- Modeled structures show an accretionary fold and thrust belt, wrapping around the northern edge of an obducted northern margin of Siletzia.
- Interpreted structures suggest the Seattle fault could have an earliest Eocene history as a tear fault within the fold and thrust belt.

Abstract

Detailed understanding of crustal components and tectonic history of forearcs is important, due to their geological complexity and high seismic hazard. The principal component of the Cascadia forearc is Siletzia, a composite basaltic terrane of oceanic origin. Much is known about the lithology and age of the province. However, glacial sediments blanketing the Puget lowland obscure its lateral extent and internal structure, hindering our ability to fully understand its tectonic history and its influence on modern deformation. In this study, we apply map-view interpretation and two-dimensional modeling of aeromagnetic and gravity data to the magnetically stratified Siletzia terrane revealing its internal structure and characterizing its eastern boundary. These analyses suggest the contact between Siletzia (Crescent Formation) and the Eocene accretionary prism trends northward under Lake Washington. North of Seattle, this boundary dips east where it crosses the Kingston arch, while south of Seattle the contact dips west where it crosses the Seattle uplift. This westward dip is opposite of the dip of the Eocene subduction interface, implying obduction of Siletzia upper crust at this location. Elongate pairs of high and low magnetic anomalies over the Seattle uplift suggest imbrication of steeply-dipping, deeply-rooted slices of Crescent Formation within Siletzia. We hypothesize these features result from duplication of Crescent Formation in an accretionary fold-thrust belt during the Eocene. The active Seattle fault divides this Eocene fold-thrust belt into two zones with different structural trends and opposite frontal ramp dips, suggesting the Seattle fault may have originated as a tear fault during accretion.

Plain Language Summary

The Puget Lowland of Washington State contains several potentially dangerous seismic faults, including the Seattle fault, which runs south of downtown Seattle. To accurately assess the earthquake hazard in this region, we need to understand the architecture and geologic history of the rocks that host these faults, deep below the Puget Lowland. We do this by using small changes in Earth's gravity and magnetic fields to create images of the Earth's subsurface. These rocks formed in a subduction zone 50 million years ago when a set of volcanic islands, similar to modern day Iceland, collided with the edge of North America. This added a layer of rock to the continent called Siletzia. We show that as the islands piled up, they broke and folded into mountain ranges. South of Seattle, Siletzia was pushed up and over ancient North America, while to the north Siletzia was pulled down and under the continent. We argue that a tear in Siletzia between these two zones eventually became the Seattle fault, giving a story for the Seattle fault's origin and early history. Our images also provide information that can improve models of ground shaking from future earthquakes affecting the greater Seattle urban area.

1 Introduction

The tectonic history of Siletzia and the location of its eastern boundary (herein termed Siletzia eastern boundary or the SEB) beneath the Cascadia forearc is a long-standing problem. It is of continuing tectonic interest because the accretion of Siletzia was a significant event in the assembly of the western margin of North America, and the history of Siletzia bears on the evolution and dynamics of the Farallon plate. Historically, there have been two prominent hypotheses that explain the origin of Siletzia; it may be an ocean island chain (Snavely et al., 1968) that was accreted to North America (Duncan, 1982) or it may have formed by forearc extension and was then consolidated to North America by a transition of the plate boundary from extensional to compressional subduction (Wells et al., 1984). These ideas have been under new scrutiny as scientists test these hypotheses with new data, including revised and refined plate tectonic circuits (McCrory and Wilson, 2013) and compilations of ongoing geologic mapping and development of detailed, more precisely dated regional stratigraphy (Wells et al., 2014).

Scientific interest in the SEB also stems from the need to define active crustal structures and crustal lithologies that impact the seismic hazard of the densely populated Puget-Willamette Lowland (e.g. Parsons et al., 1999; Blakely et al., 2002). At present, clockwise rotation of Oregon (McCaffrey et al., 2007; McCaffrey et al., 2013) deforms western Washington against the immobile Canadian Coast Mountains "backstop", producing east-trending reverse faults and northwest- and northeast-striking shear faults in the Puget Lowland (McCaffrey et al., 2007; McCaffrey et al., 2013; Wells et al., 1998). These faults, including the Seattle fault and the Southern Whidbey Island fault (SWIF) are seismically active and have documented Holocene surface ruptures (e.g. Nelson et al., 2003). These faults are superimposed on the SEB, which may create strong contrasts in crustal rheological properties that are sub-parallel to active structures in the current subduction regime. The distribution of rock types and geometries of boundaries between rock packages in the crust can affect wave propagation, and thus influence predictions of strong ground motions from a major earthquake. Therefore, understanding the basement structure beneath the Puget Lowland is fundamental to understanding the kinematics, dynamics, and seismic response of the current active fault network.

In the Puget Lowland, the location, geometry, and significance of the SEB within the Paleogene continent are poorly understood. Johnson (1984) speculated that the SEB was a north-striking dextral slip fault associated with marginal rifting (e.g. Wells et al., 1984) that is now buried beneath the eastern Puget Sound. Finn (1990) placed the boundary by identifying a sinuous gradient in the gravity anomaly map centered around 123° W longitude. Parsons et al. (1998) and Snelson (2001) inferred a boundary in the vicinity of Lake Washington from seismic tomography data, and more recently Merrill (2020) placed the boundary slightly east of Lake Washington from double-difference tomography. Using seismic tomography from EarthScope's USArray, Schmandt and Humphreys (2011) documented a high velocity "curtain" extending from the eastern edge of the Cascades to central Idaho. They interpreted this high-velocity body as a relict Farallon slab contiguous with Siletzia, a possibility supported by high velocities in the lower crust extending into eastern Washington and northeast Oregon (Gao et al., 2011), but they did not establish the location of the SEB in the upper crust. Although these studies have provided basic constraints on the location of the SEB, details of its geometry and structural evolution beneath the Puget Lowland are lacking.

In this paper, we examine the nature and extent of Siletzia in the Puget Lowland, detail the geometry of its boundary with the North American continent, and interpret the likely constituents of the Paleogene margin of the continent beneath the Puget Lowland. Due to the absence of extensive bedrock outcrop and the cover of Quaternary deposits throughout the Puget Lowland, we utilize aeromagnetic and isostatic residual gravity data to define mid- to upper-crustal structures. We measure physical properties (density and magnetic susceptibility) of Crescent basalts and the western mélange belt (WMB) that inform our map-based aeromagnetic and gravity interpretations and give us baseline values for constructing two-dimensional models based on these potential field anomalies. From the structural relations expressed in these models, we favor an early history of margin-normal compressional shortening via a fold and thrust belt during Siletzia's accretion. We attribute this intense deformation, in part, to obduction of the upper crust of Siletzia onto the North American continent.

2 Geologic Setting

Siletzia is a Paleogene oceanic basalt terrane forming the basement of the Cascadia forearc in Washington, Oregon, and Vancouver Island, Canada (figure 1; McCrory and Wilson, 2013; Wells et al., 2014). Siletzia consists of the Crescent Formation in Washington (figure 2), Siletz River Volcanics in Oregon (Snavely et al., 1968; Snavely et al., 1993; Wells et al., 2014), and the Metchosin Igneous Complex on Vancouver Island (Massey, 1986; Muller, 1980). Exposures of Siletzia are largely restricted to Neogene uplifts in the forearc, where it consists dominantly of tholeiitic pillowed and subaerial basalt ranging in age from 56 to 49 Ma (Wells et al., 2014). Seismic-reflection profiles show that high-velocity mafic crust of Siletzia thickens southward, from ~7-10 km on Vancouver Island (Hyndman, 1995) to a maximum of 33-35 km in central Oregon (Fleming and Trehu, 1999; Trehu et al., 1994). In the Olympic Mountains, its base is in thrust contact with the underlying Oligocene to Holocene accretionary complex of the Olympic Mountains to the west (Tabor and Cady, 1978a).

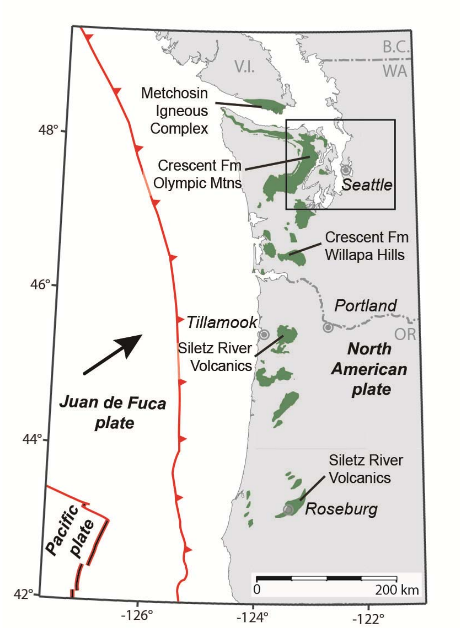

Figure 1

Figure 1. Tectonic setting for study area. Box shows the study area and extent of the map in figure 2. Hachured line is the trench between the North American and Juan de Fuca plates; double lines show a spreading zone between the Pacific and Juan de Fuca plates. Arrow shows motion direction of the Juan de Fuca plate relative to North America. Green polygons show outcrops of Siletzia in the Coast Ranges.

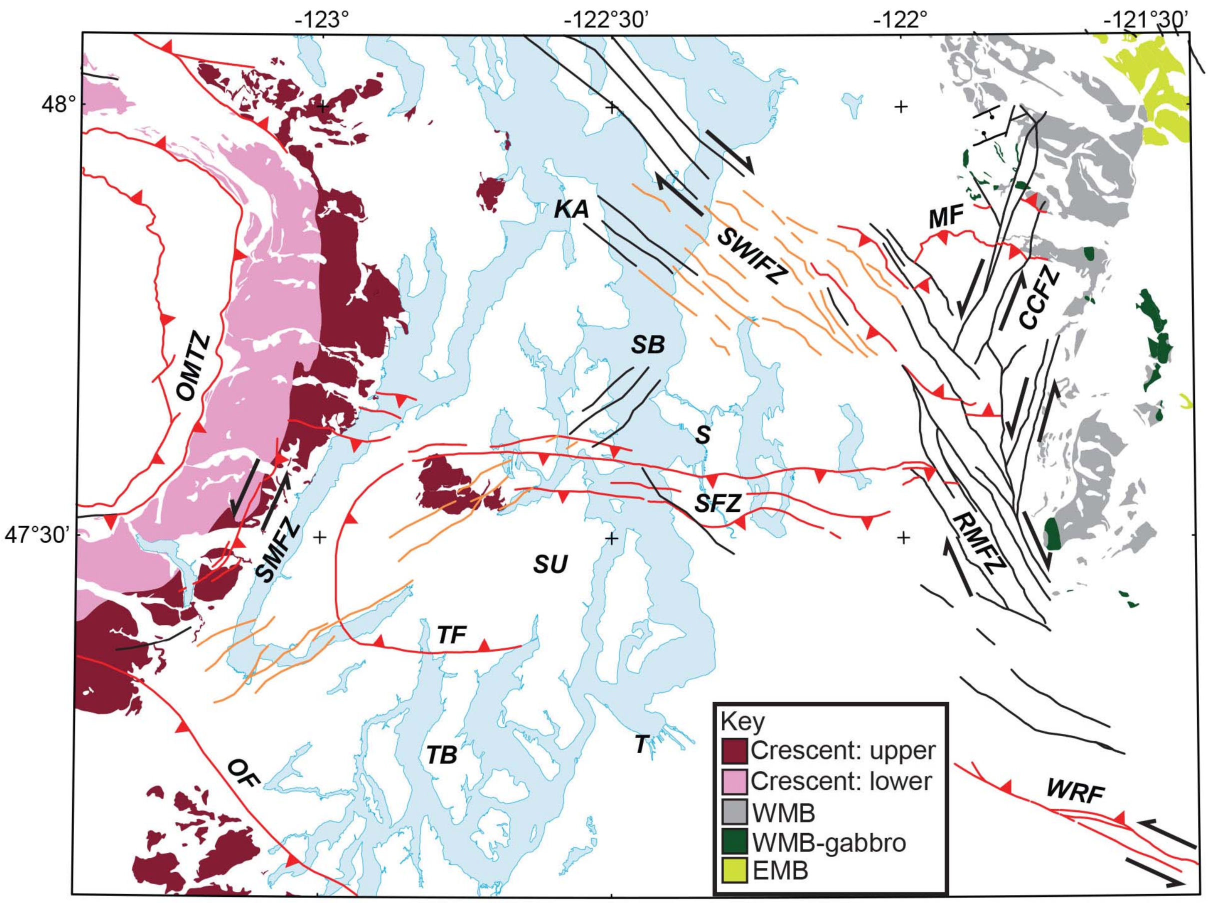

Figure 2

Figure 2. Regional fault map of the Puget lowland region with distribution of basement rock outcrops for the Crescent formation and the Western/Eastern mélange belts. Box in figure 1 outlines the regional location. Major through-going faults of Eocene to recent age are color-coded by type: red = dominantly thrust or reverse faults; black = dominantly strike-slip or normal faults; orange = faults with unknown slip sense identified from aeromagnetic lineaments. CCFZ = Cherry Creek fault zone; KA = Kingston Arch; MF = Monroe fault; OF = Olympia fault; OMTZ = Olympic Mountains thrust zone; RMFZ = Rattlesnake Mountain fault zone; S = Seattle; SB = Seattle Basin; SFZ = Seattle fault zone; SMFZ = Saddle Mountain fault zone; SWIFZ = Southern Whidbey Island fault zone; SU = Seattle Uplift; T = Tacoma; TB = Tacoma Basin; TF = Tacoma fault; WRF = White River fault (Blakely et al., 2009; Czajkowski and Bowman, 2014; Dragovich et al., 2014; Lamb et al., 2012; Mace and Keranen, 2012; Sherrod et al., 2008; U.S. Geological Survey, 2006). Blue polygons outline major waterways.

Where exposed on Vancouver Island and near Roseburg, Oregon, the SEB is a reverse fault contact (Clowes et al., 1987; Wells et al., 2000). Siletzia was clearly deformed into a fold and thrust belt during accretion at Roseburg, and sedimentary onlap documents accretion by 50 Ma (Wells et al., 2014). On Vancouver Island and at Roseburg, Siletzia is reverse faulted beneath an older Jurassic and Cretaceous accretionary complex. On Vancouver Island, this complex was exhumed at about 45 Ma, presumably during Siletzia's accretion (Groome et al., 2003). In the Cascade foothills east of the Puget Lowland, the WMB contains similar Mesozoic accretionary rocks, but there and everywhere within the 600 km region between Roseburg and Vancouver Island, the location of the terrane boundary is buried beneath the volcanic arc and post accretion sediments, therefore timing and structure are difficult to ascertain.

3 Methods

3.1 Potential field data

Gravity data for the Puget Lowland are from the state database of Finn et al. (1991), with additions from Walsh (1984), Blakely et al. (2007), Robert Morin and Victoria Langenheim (written communication), and ~750 stations that we collected between 2006 and 2012 (Supporting Information: Gravity data and methods S1). We reduced the data to isostatic residual gravity anomalies to focus on upper-crustal structure (figure 3; Supporting Information: Gravity data and methods S1). Aeromagnetic data used in this study (figure 4) were acquired in 1997 via low-flying aircraft with a stinger-mounted magnetometer (for additional details see Blakely et al., 1999). North-south flight lines are ~0.4 km apart, with east-west tie lines spaced at 8 km. Aeromagnetic measurements were interpolated to a projected, rectilinear grid using the bi-directional gridding algorithm provided in Oasis Montaj (Geosoft, 2016). Bi-directional gridding is appropriate for data collected along parallel or roughly parallel lines (Geosoft, 2014).

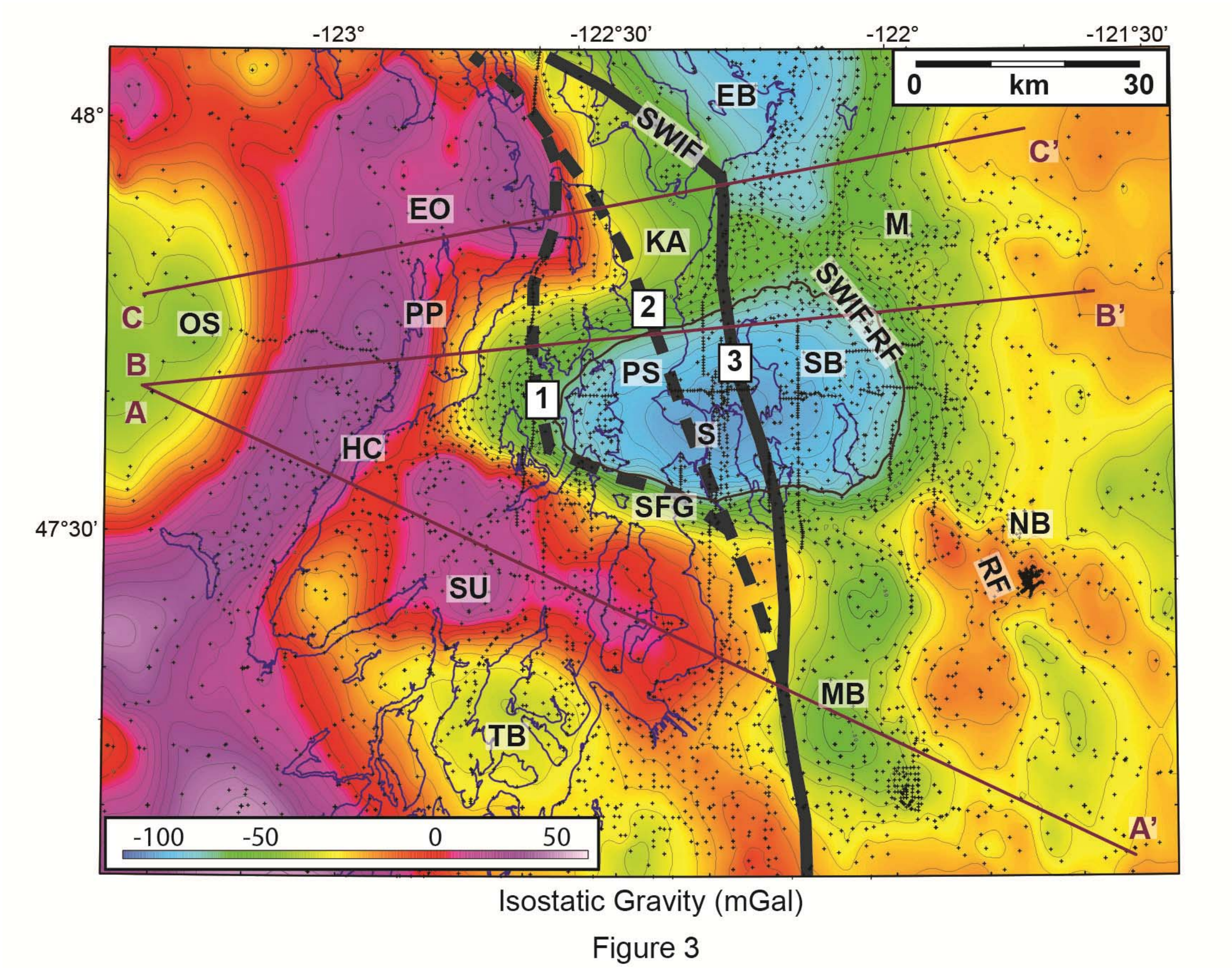

Figure 3. Isostatic residual gravity in milligals (mGal) for the Puget Lowland. Box in figure 1 outlines the regional location. Contour interval is 5 mGal, and small crosses show location of data points constraining the gravity grid. The bold contour is discussed in the text. Waterways are outlined by blue lines. Brown lines show locations of models in figures 8, 9 and 10 (A-A', B-B', and C-C', respectively). Thick, grey lines show potential locations of the Siletzia eastern boundary referenced in the text; the solid line (3) indicates the most likely position. EB = Everett basin; EO = small Eocene basin; HC = Hood Canal; KA = Kingston arch; LC = Lower Crescent; LW = Lake Washington; M = Monroe; MB = Muckleshoot basin; MP = Mt. Persis formation aeromagnetic high; NB = North Bend; OS = Olympic sedimentary core; PP = Pulali Point; PS = Puget Sound; RF = Rattlesnake Mountain fault zone; S = Seattle; SB = Seattle basin; SFG = Seattle fault gravity gradient; SU = Seattle uplift; TB = Tacoma basin; UC = Upper Crescent; WMB = Western mélange belt.

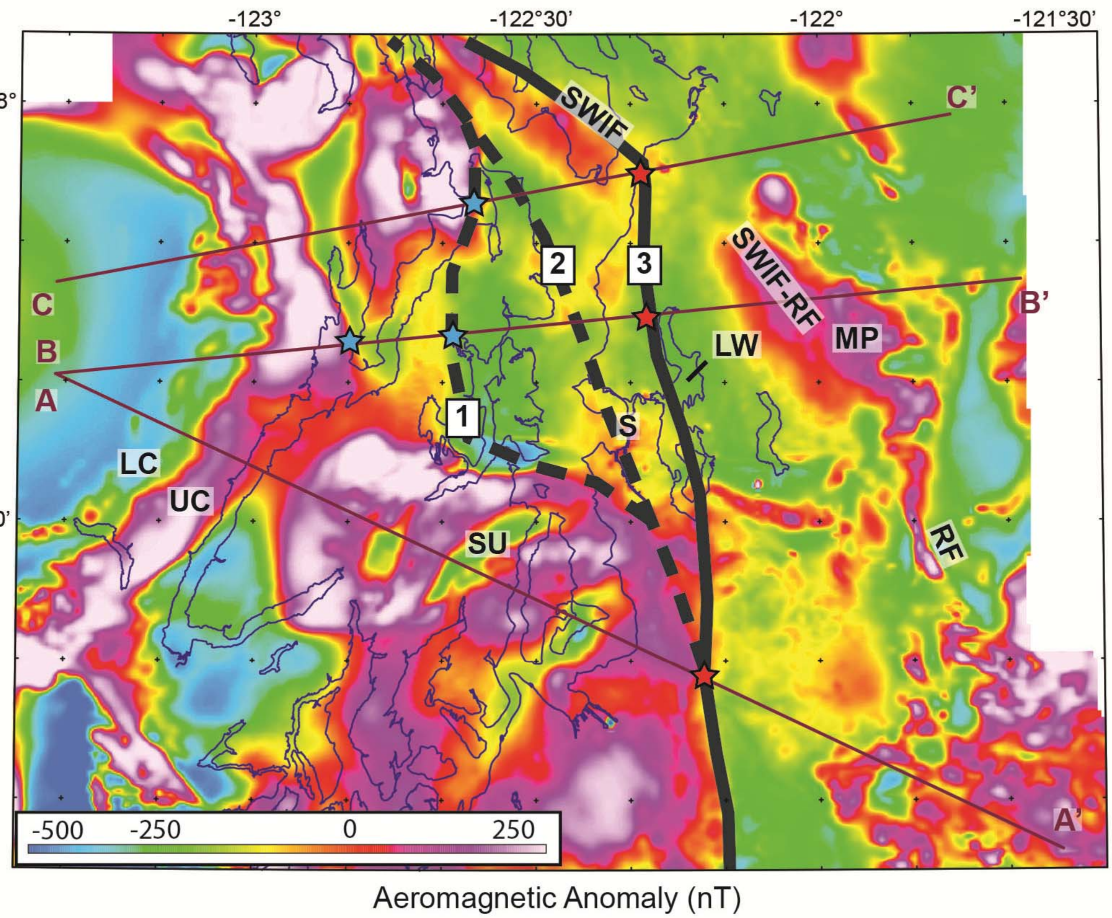

Figure 4

Figure 4. Reduced-to-pole aeromagnetic anomaly in nanoteslas for the Puget Lowland. Box in figure 1 outlines the regional location. Most other notations as in figure 3. Red and blue stars show the location of red and blue arrows shown in figures 8-10.

3.2 Pseudogravity filter

We mapped the lateral extent of the Crescent Formation by transforming the aeromagnetic data to pseudogravity anomalies (also termed "magnetic potential; figure 5). This transformation is a linear filter applied to total-field magnetic anomalies in the Fourier domain (Blakely, 1995). It effectively replaces the distribution of magnetization causing the magnetic anomaly with a proportional density distribution, thereby giving magnetic anomalies the mathematical properties of a gravity anomaly. We used the pseudogravity algorithm provided by Oasis Montaj (Geosoft, 2016). In our application, pseudogravity anomalies have three advantages over magnetic anomalies (Blakely, 1995). First, the pseudogravity transformation eliminates magnetic anomaly skewness caused by nonvertical magnetization and ambient field, thereby centering anomalies over their causative sources. Second, pseudogravity anomalies have steepest horizontal gradients located approximately over the edges of causative sources, facilitating our mapping of lithologic contacts. Third, the pseudogravity transformation enhances anomalies caused by deeper sources, particularly useful in mapping fundamental midto lower-crustal and mantle boundaries. To define the potential lithologic boundaries, we compute the maximum horizontal gradient of the pseudogravity anomalies (figure 5).

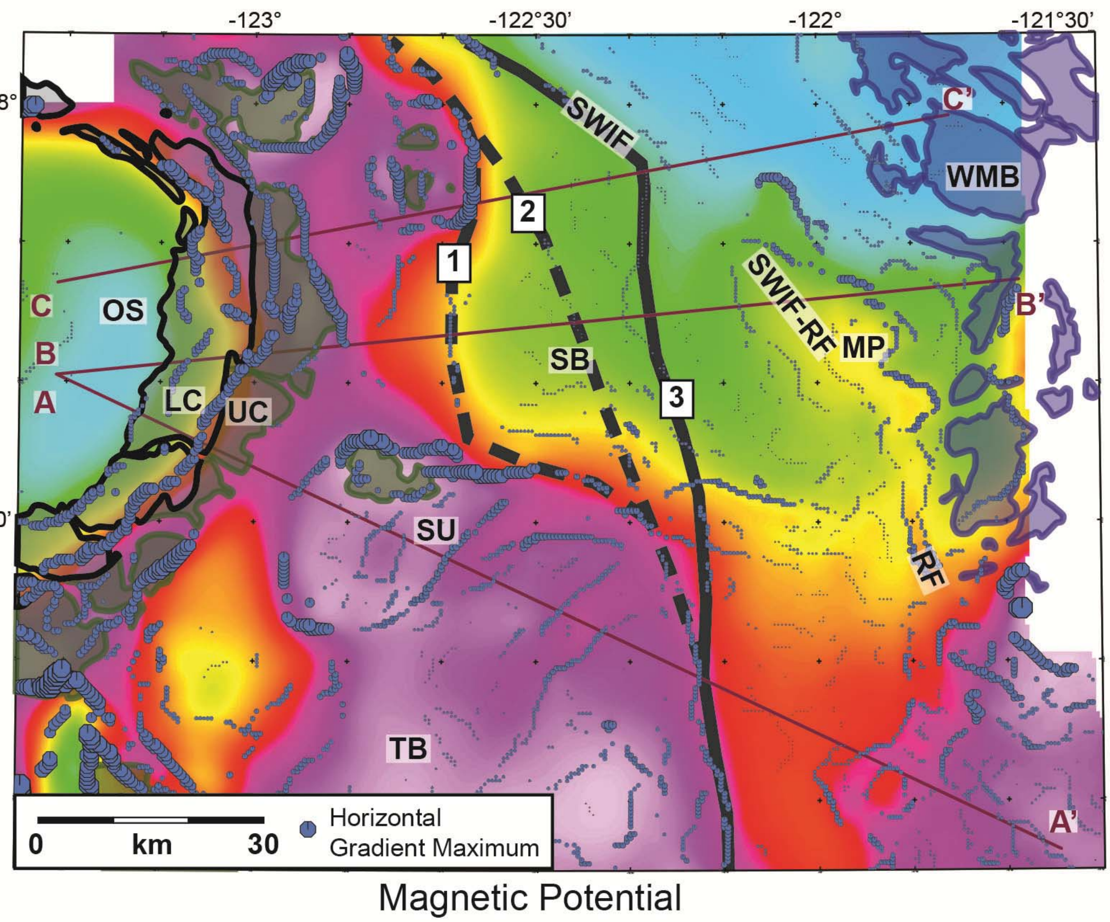

Figure 5

Figure 5. Pseudogravity (magnetic potential) computed from the regional aeromagnetic anomaly for the Puget Lowland. Box in figure 1 outlines the regional location. Warm colors are high and cool colors are low values; color bar not included due to the lack of physical meaning for the units. Lightly shaded black outlines show approximate extent of lower Crescent formation exposures in the western half of the map, and green outlines show the extent of upper Crescent exposures. Lightly shaded blue outlines in the eastern half of the map show the approximate extent of the western and eastern mélange belt outcrops. Blue dots show locations of maxima in the horizontal gradient of the pseudogravity scaled to the strength of the gradient. All other notations as in figure 3.

3.3 Rock physical properties

Physical property measurements are available for rock formations in the Puget Lowland area through prior sampling, sonic logs from wells, and prior geophysical modeling (Blakely et al., 2009; Brocher and Christensen, 2001; Brocher and Ruebel, 1998; Finn, 1990; Sherrod et al., 2008). We supplemented these existing measurements with extensive sampling of mapped units in the western part of the Puget Lowland and from detailed geologic mapping in the eastern portion of the Puget Lowland (Anderson et al., 2011; Dragovich et al., 2007, 2008, 2009, 2010a, 2010b, 2011a, 2011b, 2012, 2013). Physical property data and methods S2 of the Supporting Information describes lab measurements of rock densities and lab and outcrop measurement of rock magnetic susceptibility. Sample measurements generally represent a minimum density because rocks (especially sedimentary rocks), are compacted by lithostatic pressures at depth. Magnetic susceptibility of hand samples and outcrops also represent minimum values because weathering alters magnetic minerals in near-surface exposures.

3.4 Two-dimensional forward modeling of potential field anomalies

We collected closely-spaced gravity data along a WNW-trending line (figure 3, line A-A') across the long axis of the Seattle uplift, a place where deeper boundaries expressed in the potential field anomalies would not be buried by upper crustal basins. We augment this fundamental 2-D model line with two additional 2-D models (figure 3, lines B-B' and C-C') across zones with closely-spaced previously existing gravity data and detailed, high-quality geological mapping predominantly at a scale of 1:24,000. Together, the three lines allow us to extrapolate the SEB location through the Seattle basin, Kingston arch, and southern Everett basin.

We utilize both isostatic residual gravity anomalies and aeromagnetic anomalies to constrain 2-D forward modeling using GMSYS (Geosoft, 2016). The model profiles lie approximately perpendicular to mapped potential-field gradients that identify the SEB. Heights above land surface for the aeromagnetic flight lines were measured with in-flight radar. Our models are floored at 20 km depth for two reasons. First, isostatic anomalies are insensitive to geologic boundaries below mid-crustal level. Second, models constructed with Bouguer gravity anomalies in the Puget Lowland suggest insensitivity of gravity data in this particular region to structures below ~20 km (Snelson, 2001) to 50 km (Finn, 1990).

The modeling process, illustrated for the Seattle uplift (figures 3-5), involves rigorous testing of a wide variety of geologically plausible possibilities for crustal structure that still fit constraints provided by mapped formations at the surface, measured rock properties for different formations (Supporting Information: Physical property data and methods S2), available well data, and structures imaged by active and/or passive source seismic data. Due to the interactive nature of the forward modeling software, quantifying the number of completed tests and/or quantifying all uncertainties is difficult. Therefore, we describe and illustrate our approach and subsequently discuss in more detail uncertainties for structural parameters most critical for our interpretation of the results in terms of kinematic tectonic processes (a wide range of models with a variety of misfit are available in the Supporting Information figures S1-8). At the start of the process, models are as simple as possible and focus on deeper boundaries. We test boundary position (figure 6) and dip (figure 7) against broad trends in both the gravity and magnetic data, then move the best fit model forward by adding finer details near the surface (figure 8). We add a thin veneer of undifferentiated Quaternary glacial deposits over regions where it is mapped at the surface. Where active seismic data constrain deeper structures, we estimate densities via established relationships between seismic velocities and densities for earth materials (Brocher, 2005; Gardner et al., 1974). Elsewhere, we use the depth-density relationships for compaction of sedimentary rocks from general studies (Gardner et al., 1974) and local well data (Brocher and Christensen, 2001; Brocher and Ruebel, 1998) using our lab measurements as a starting point.

Structure on the west end of each line (across the Olympic Mountains) is well constrained by surface exposure of fundamental crustal units (figure 2) and associated physical property measurements. Unit structural geometries at depth in this region are less certain, although fold geometries that work for our data are similar to other published studies across the western Olympic Mountains (Blakely et al., 2009; Lamb et al., 2012). Therefore, we chose the western end of each model line as our datum, tying the gravity and magnetic data to the model computation.

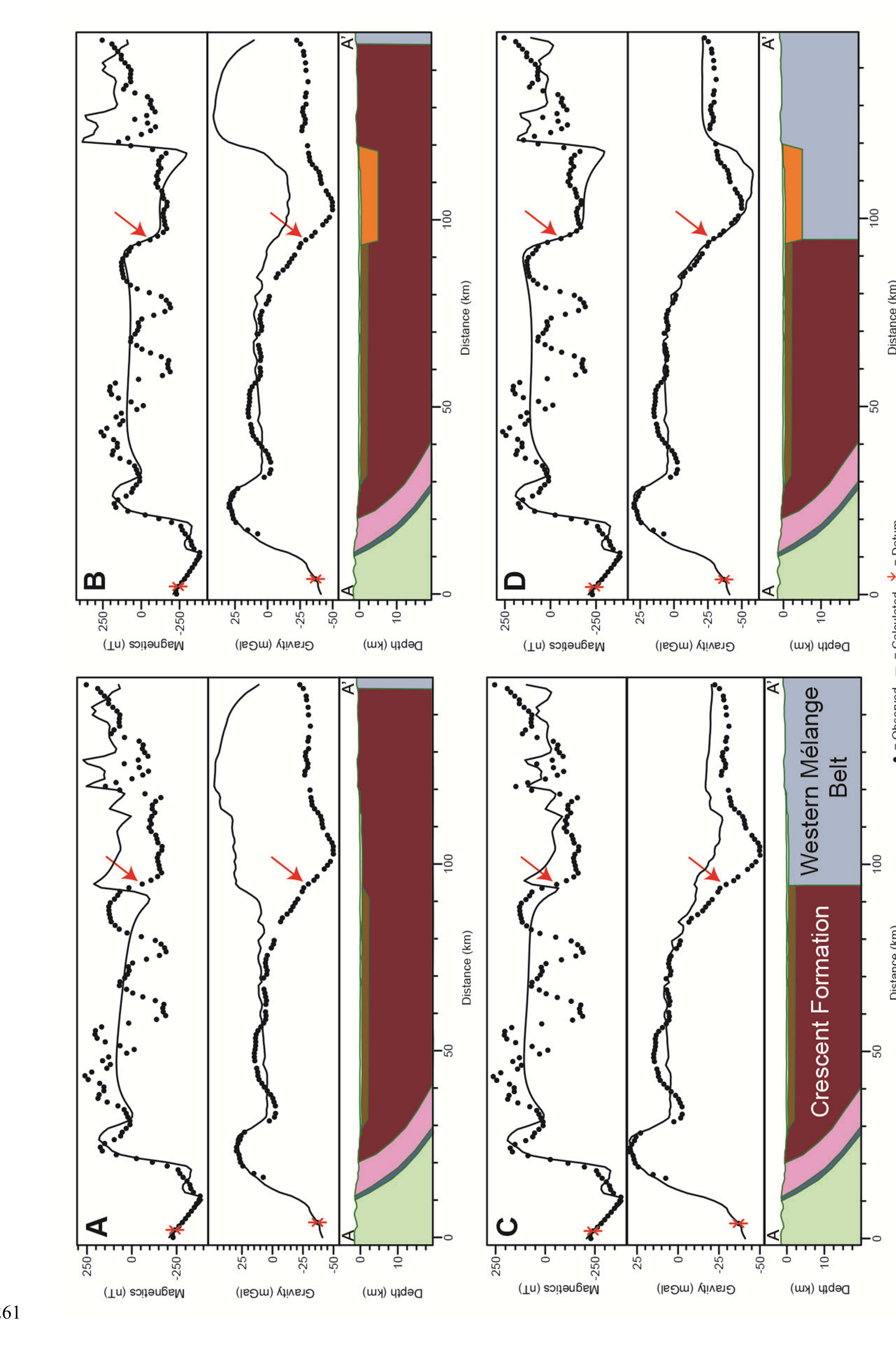
A
B
C
D
Magnetics (nT)
Gravity (mGal)
Depth (km)
Distance (km)
A
A'
Crescent Formation
Western Mélange Belt
• = Observed — = Calculated = Datum

Figure 6

Figure 6. Example of the modeling process for line A-A' (see location in figures 3-5). Top panel in each example shows data (dots) and model prediction (line) for the aeromagnetic anomaly (not reduced to pole); middle panel shows isostatic residual gravity anomaly data and model prediction; bottom panel shows the model. Red arrow shows the position of prominent gradients defining the location of the eastern boundary of Siletzia. The datum ties the model to the data in a position where the subsurface geology is best understood. Colors correspond to geologic units as listed in table 1. a) Extending Siletzia across the entire Puget lowland poorly fits the gravity data. b) Including a low density and low susceptibility Muckleshoot basin greatly helps to fit the magnetic data. c) Including a boundary in the middle of the Puget Lowland greatly helps fit the gravity data. e) This rather simple model including both a basin and a mid-Puget Lowland boundary comes surprisingly close to matching the gravity and magnetic gradients highlighted by the red arrows.

	Density		Magnetic Susceptibility	
	Average	Range	Average	Range
Basement Rocks				
Western Melange Belt Metasedimentary	2720		12	0.8-30
Western Melange Belt Metagabbro	2840		50	
Crescent Basalt-Upper	2816	2790-2840	41	23-65
Crescent Basalt-Lower	2836	2790-2890	10	0-19
Blue Mountain Unit	2660		0.3	0-0.5
Olympic Core Rocks	2680		0.5	
Basin Fill				
Eocene Aldwell and Equivalent Units	2440	2420-2480	0.6	
Muckleshoot Sediment-Lower	2610	2550-2670	4.5	0-9
Muckleshoot Sediment-Upper	2430		0	
Blakely Formation and Miocene Sediments	2207	2140-2240	0	
Quaternary Glacial Cover	2057	2010-2080	0	
Cascades-Related Volcanics				
Volcanic Rocks of Mt. Persis-Basalt	2700		80	
Volcanic Rocks of Mt. Persis-Volcaniclastic	2468	2400-2570	49	3-70
Miocene and younger Cascades Volcanics	2524	2500-2570	28	10-50

Table 1

Table 1. Geologic formations utilized in the modeling process with corresponding colors (as depicted in figures 8-10) and physical properties. Densities are in kg/m^3 and magnetic susceptibility in SI x 10^{-3}. Properties are based on field and lab sample measurements as described in the Supporting Information: Physical property data and methods S2. A range of values is given where there is variation in properties outcrop to outcrop, and thus allowable variation in the corresponding model values.

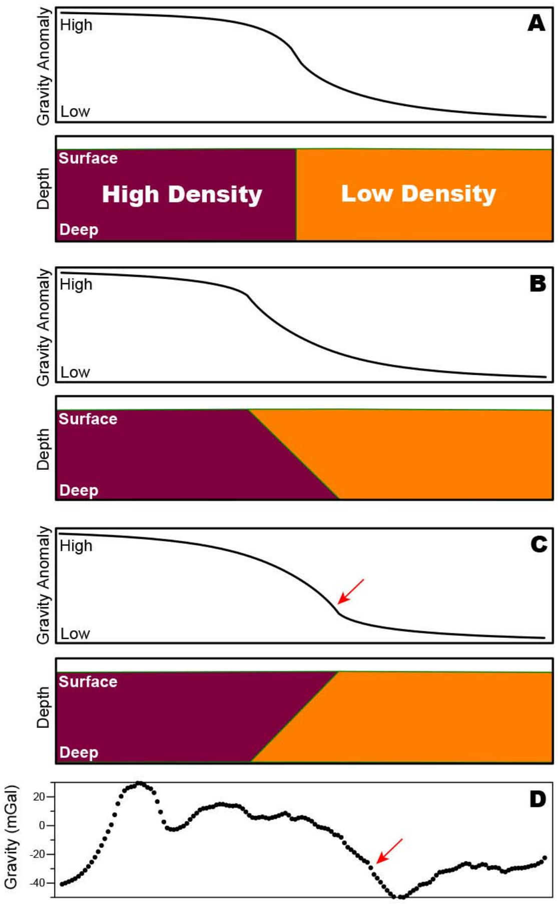

Figure 7

Figure 7. Simple models showing examples of faults with different dips. a) Vertical boundary. The resulting anomaly (top panel) is symmetrical, with the greatest gradient above the fault location. b) Dipping boundary with low density rocks above high density rocks. The anomaly is asymmetrical and concave up with the greatest gradient near the intersection of the boundary with the surface. c) Dipping boundary with high density rocks above low density rocks. The anomaly is asymmetrical and convex up with the greatest gradient near the intersection of the boundary with the surface. e) Data from the Seattle uplift profile (figure 8), highlighting the convex upward shape of the gradient with the maximum gradient shown with a red arrow, similar to model (c).

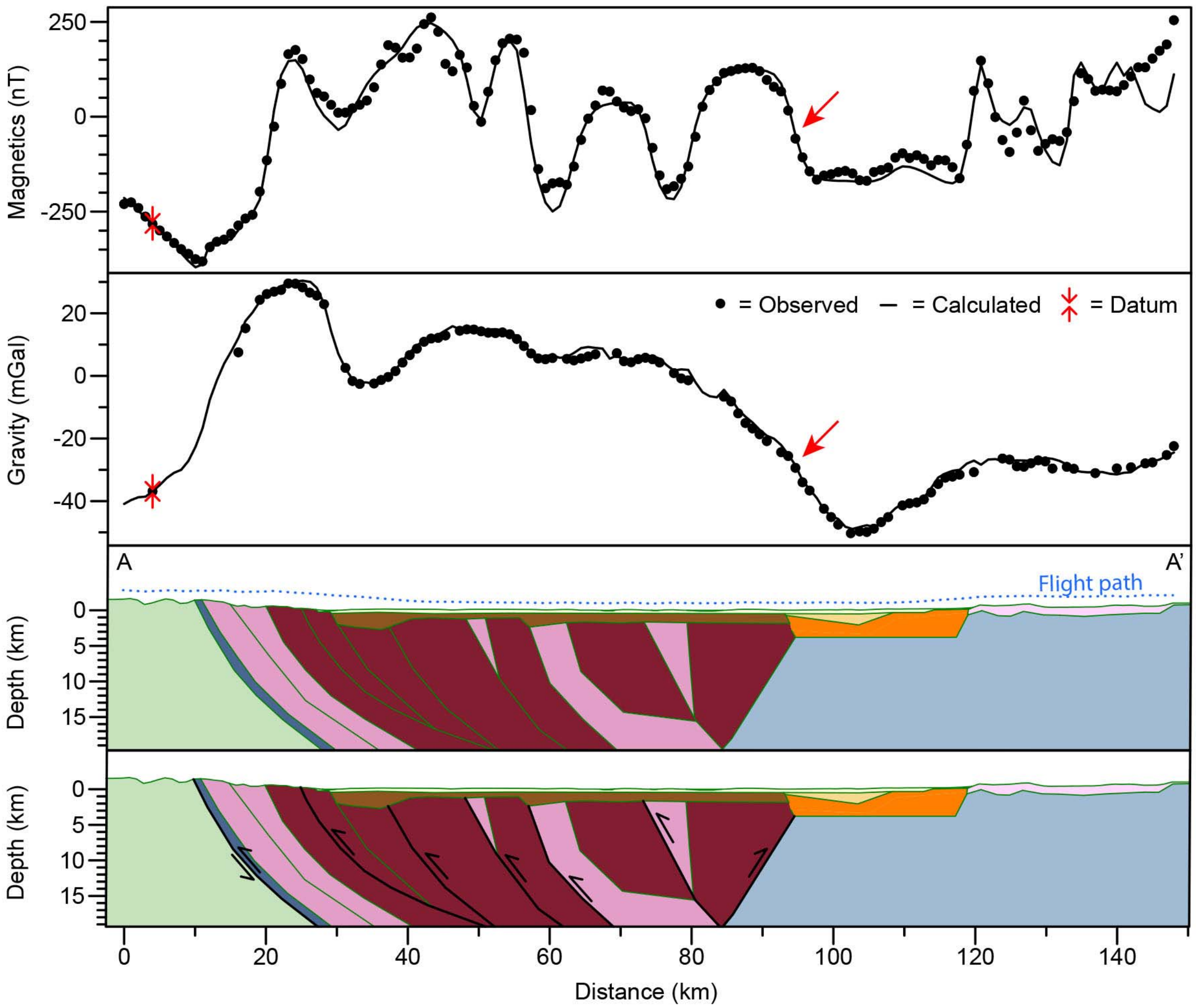

Figure 8

Figure 8. Best-fit model for Seattle uplift and associated interpreted thrust structure. The structural model shown in the bottom panel predicts the gravitational and magnetic anomalies shown by the black lines in the upper two panels. Colors correspond to geologic units as listed in table 1. Other details are described in the caption for figure 6. Red arrows show the position of the gradients interpreted as defining Siletzia's eastern edge (SEB), also shown in map view in figure 4. Note that the details of Cascades volcanics blanketing the eastern end of this model and models shown in figures 8-9 are too small to appropriately model at this scale, therefore fit of magnetic data in this location is only approximate, but more carefully addressed in the Monroe, Carnation, and Lake Joy 7.5' quadrangles (Dragovich et al., 2008, 2010b, 2012).

We note that there is some variability in the magnetization and density of the Olympic core sediments, especially just west of our profiles. However, the influence is minor and largely affects the overall base level values of anomalies on the profile line, whereas the shape of these anomalies directly relate to modeled units below the profile itself. Our crustal models also do not include any component of reversed remanent magnetization for the Crescent Formation. This is based on 1) strong observed correlations between measured variations of magnetic susceptibility of Crescent Formation units and aeromagnetic anomaly patterns in the Olympics (Blakely et al. 2009), and 2) observations that Siletzia's pillow basalt typically has a substantial normal overprint that masks a reversed remanence (e.g., Wells and Coe, 1985). Alternative interpretations are discussed below.

4 Where is the Eastern Edge of the Crescent Formation?

4.1 High and low anomalies

Large-scale pseudogravity and isostatic gravity high anomalies broadly correlate with Crescent Formation exposures (figures 3 and 5). High magnetic susceptibility and density measurements of the Crescent Formation support this correlation (Table 1). The Crescent Formation is in fault contact with the interior of the Olympic Mountains.Surface exposures of Eocene-Miocene marine sediments show the core of the Olympics are an accretionary complex (Tabor and Cady, 1978a). This complex corresponds to a zone of low magnetic and isostatic anomalies (OS in figures 3 and 5), in accordance with our measured low densities and magnetic susceptibilities for these core units (Table 1).

Isostatic gravity and pseudogravity lows along the eastern side of the Puget Lowland (figures 3 and 5) spatially correlate with the relatively lower density and magnetic susceptibility of WMB rocks compared to Crescent Formation (Table 1). Therefore, we subdivide Puget Lowland basement into two lithologies: Crescent basement and WMB, excluding the core of sedimentary rocks in the Olympic Mountains from either type. Prior geophysical studies used terms such as Cascade basement or Cascade crust to refer to the eastern Puget Lowland basement source of typically lower amplitude magnetic and gravitational anomalies and low P-wave velocities (Finn, 1990; Snelson et al., 2007). We call the basement by its formation name, leaving the more general Cascades basement term for unknown basement lithologies farther east under the arc.

We see aeromagnetic variations over exposed Crescent Formation, indicating it is variably magnetized. A particularly clear example is Crescent Formation along the southeastern edge of the Olympic Mountains where upper and lower member basalts are exposed at the surface, thus correlation with potential field anomalies is straightforward. Here, the upper member of the Crescent Formation (Tabor and Cady, 1978a; UC in figure 5) has high magnetism distinct from the less magnetic lower member (LC in figure 5; also visible in figure 4). This division in the magnetic character of the Crescent Formation was previously noted by Hirsch and Babcock (2009) and Blakely et al. (2009).

Low aeromagnetic anomalies over the lower-member Crescent Formation in the Olympic Mountains may be caused either by rocks with low magnetic susceptibilities (as modeled in the Olympics by Blakely et al., 2009) or by reversed remanent magnetization (as modeled across the Seattle uplift by Hagstrum et al., 2002). Physical property measurements on Olympic peninsula Crescent Formation exposures suggest aeromagnetic lows are caused by low magnetic susceptibilities. Magnetic susceptibility measurements of Crescent basalt show high susceptibility on average for the upper member of the Crescent Formation and lower susceptibility for the lower member (Blakely et al., 2009; Table S2). Heterogeneous chemical and hydrothermal alteration and/or metamorphism may explain the variation in magnetic susceptibility for the Crescent Formation. For example, there are distinct chemical differences between the upper and lower parts of the formation (Babcock et al., 1992). Burial metamorphism to lower greenschist facies in the lower part of the 16 km-thick section (Glassley, 1974; Hirsch and Babcock, 2009; Warnock et al., 1993) may be a likely explanation for these variations. We prefer to apply this strong relationship to our data across the Puget Lowland, but acknowledge that a component of reversed magnetization is possible. Aeromagnetic anomaly variations similar in amplitude to the southeast Olympics are obvious within the aeromagnetic data for the Seattle uplift (SU in figures 4 and 5). We hypothesize this variation is due to structure within the basement creating a repeating stack of sections of upper and lower member Crescent Formation, explored further with our modeling below.

Over the Crescent Formation, some strong variations in total field aeromagnetic anomalies persist when filtered to pseudogravity anomalies, indicating that magnetization variations are deep-seated. This is not the case over all volcanic rocks of the Puget Lowland. For example, a high-amplitude magnetic anomaly over a mapped zone of the Volcanic Rocks of Mount Persis (MP, figures 4 and 5) is diminished in pseudogravity anomalies, suggesting that this magnetic anomaly is caused by near-surface rocks.

Though the pseudogravity analysis helps us focus attention on deeper magnetic source rocks, zones of basin sediments reaching into the mid-crust do have an influence on the pseudogravity computation; for instance, the area over the Seattle basin (SB in figures 3 and 5) is a relative low on the pseudogravity map. It can be hard to see basement anomalies "through" deep basins, even with the pseudogravity computation (for an example of this effect, see Supporting Information figure S1), which is discussed further below. Oddly, the Tacoma basin (TB in figures 3 and 5) does not coincide with an equivalent low on the pseudogravity map. While the Tacoma basin is much shallower (~2-6 km) than the Seattle basin (~7-9 km) (Brocher et al., 2001; ten Brink et al., 2002), it should have some effect. The lack of a Tacoma basin pseudogravity low could be due to A) anomalous ultramafic rocks in the crust under the basin (Steely et al., 2021), B) thick, magnetic volcanics filling a substantial portion of the basin (Polenz et al., 2021) or C) a cold, hydrated, magnetic mantle wedge below the southwestern and west central Washington (Blakely et al., 2005). These multiple possible interpretations cast some uncertainty on the influence of large basins on the pseudogravity map, so we test and discuss several possibilities for the extension of the Crescent/WMB basement boundary under the Seattle basin.

4.2 Gradients between anomalies

Potential field data are best used to define lateral contrasts between subsurface geologic units across vertical or steeply dipping boundaries. A lateral transition from the Crescent Formation to the WMB basement will create gradients in pseudogravity and gravity maps. Due to the concealing effects of younger basins, the best place to look for such gradients is along the east-west transect over the Seattle uplift (line A-A', figures 3-5). Several linear, northeast-trending pseudogravity gradients do cross the Seattle uplift at and west of Puget Sound (figures 4 and 5), but another linear (and longer), north-trending gradient lies to the east of Puget Sound (figure 5, gradient #3). Though this eastern gradient is weaker than those over the uplift, its length and linearity suggest that it is the product of a fundamental, through-going crustal-scale geologic boundary. Furthermore, this pseudogravity gradient coincides with a gravity gradient with similar trend (figure 3) that separates a high gravity anomaly over the Seattle uplift from a low gravity anomaly on the eastern side of Puget Sound. This suggests that both gravity and pseudogravity gradients result from the same contact.

A similar pseudogravity and corresponding gravity gradient exists at the northernmost edge of our study area, on Whidbey Island (figure 5, gradient #3). These gradients bound the eastern edge of a magnetic anomaly with a magnitude comparable to the anomaly over the Seattle uplift. Pseudogravity anomalies over the middle of the Seattle basin, on the other hand, show only minor and not strongly linear gradients, probably because basement is deeply buried by thick basin sediments (see Supporting Information figure S1). Moreover, anthropogenic magnetic anomalies from urban development in this region overprint deep-basement anomalies (figure 4). Given the lack of basement signal over the Seattle basin, the simplest hypothesis is that the basement boundary falls near the western edge of the basin (figure 5, gradient #1), separating pseudogravity anomalies of similar amplitude as to the north and south.

Two other gradients are possible candidates for the SEB under the Seattle basin: a weak and discontinuous gradient through the middle of the basin (figure 5, gradient #2), and a weak but linear gradient that trends north through the basin and then bends westward to meet the stronger gradient in the Kingston arch region (figure 5, gradient #3). We test each possibility with two-dimensional modeling. We note that gradients #2 and 3 coincide with a transition in the character of a low gravity anomaly, the shape of which represents the extent and possibly the depth of the Seattle basin. Though it is a subtle effect, the western part of the Seattle basin appears shallower, with a less pronounced gravity low than the eastern part of the basin (figure 3). The Seattle basin also appears narrower in north-south extent in the western part of the basin compared to the east (see, for example, highlighted gravity contour in figure 3). This could result from an actual shape change in the basin from west to east, or a change in physical properties of the basement rocks from east to west.

Other bounding gradients stand out within the pseudogravity map. In particular, the north-directed reverse Seattle fault makes a strong gradient. This structure has the greatest influence on aeromagnetic anomalies in the area. The Seattle fault gradient is higher amplitude on its western end than on the eastern end (figure 5), but the gradient extends across the entire Puget Lowland region. The transition in gradient amplitude suggests that the fault bounds more strongly magnetic rocks south of the fault in the west, pointing to a transition in basement physical properties across gradient #2 or 3. The SWIF and Rattlesnake Mountain fault zone have documented neotectonic activity (e.g. Dragovich et al., 2008; Sherrod et al., 2008) and coincide with pseudogravity and isostatic gradients that are weaker than other boundaries in the region (SWIF, and RF on figures 3 and 5).

5 Anomaly Modeling: What does Siletzia Look Like at Depth?

We present three two-dimensional models that support a geometric interpretation of the structure of the Siletzia eastern boundary (SEB) as well as internal structure of Siletzia below the Puget Lowland. Geophysical gradients crossing the Seattle uplift (A-A' in figures 3-5) are more straightforward to interpret because basement is shallower here than elsewhere. A line crossing through the Seattle basin (B-B' in figures 3-5) tests different gradients possibly representing the SEB (red and blue arrows in figures 8-10; red and blue stars in figure 4). We note Snelson (2001) modeled a gravity line through the center of the Seattle basin ~10 km south of our model B-B'. Line C-C' (figures 3-5) through the Kingston arch constrains the northern segment of the SEB, clarifying its placement with respect to the SWIF.

5.1 Seattle uplift

Along the eastern end of the line crossing the Seattle uplift (A-A' in figures 3-5), Tertiary to Quaternary volcanic and sedimentary rocks cover basement rocks (Dragovich et al., 2002; Walsh et al., 1987). Active seismic data that cross onto the Seattle uplift (Pratt et al., 1997) constrain a maximum thickness of Eocene (or younger) units covering the Crescent Formation, although interpretations of thickness vary (Brocher et al., 2004; Pratt et al., 1997; ten Brink et al., 2002). Gradients in both total field magnetic and gravity anomalies (red arrow, figures 6 and 8) spatially correlate with each other and with gradient #3 identified in pseudogravity and aeromagnetic anomaly data (red star, figure 4), strongly suggesting that the SEB sources these gradients. However, just to the east of these gradients, a low velocity tomographic anomaly (Van Wagoner et al., 2002) and a gravity low are coincident with sedimentary rocks of the Muckleshoot basin (MB in figure 3). We tested multiple possibilities for modeling the magnetic and gravity gradients involving the SEB, the Muckleshoot basin, or both (figure 6 b-d), the latter of which best fits the broad trends in the data. A boundary position at the Cascades foothills creates a gravity anomaly that is too high over the eastern Puget Lowland compared to data (figure 6 a-b), therefore an SEB position at gradient #3 fits our data best along A-A'. We note that the Muckleshoot geometry is approximate, as is the density of its Miocene basin-fill sediments, but tomographic data (Van Wagoner et al., 2002) constrain its steep-sided geometry, lateral extent, and 4 km depth.

The position of the shallow (less than 5 km depth) part of the SEB strongly influences the shape of its associated magnetic gradient with the best fit corresponding to the western edge of the Muckleshoot basin (figure 6d). Therefore, we fix this portion of the model when developing more detailed interpretations (see Supporting Information figure S2 for model fit issues introduced by moving this part of the boundary). Given this constraint, we obtain a best fit to the gravity data by including a westward dip on the lower portion of the SEB along line A-A' (figure 8). Gravity data strongly preclude an eastward dip because it would predict higher gravity than observed over the region immediately west of the Muckleshoot basin (see Supporting Information figure S3). The shape of the gravity gradient also suggests a westward dip because the closely-spaced gravity measurements define a convex-up shape of the gravity gradient which is diagnostic of boundary dip (figure 7; Saltus and Blakely, 2011). Therefore, our interpretation of the westward dipping geometry of the SEB along this line is quite robust and best fits the gravity, magnetic, active source seismic, and tomographic data. Note that while a rather steeply-dipping boundary is required by the data, the exact angle of dip is not well constrained.

The model cross-section includes "slices" of less-magnetic Crescent Formation embedded within the larger unit (figure 8). These are required to fit arcuate magnetic anomaly lows trending normal to the model line (figure 4; see maximum gradient trends for the orientation of anomaly edges in figure 5). The magnetic lows could arise from narrow basins filled with thick sediment on top of more uniformly-magnetized Crescent Formation, but this hypothesis is not borne out by our modeling (see Supporting Information figure S4); smooth and consistently high gravity values across the Seattle uplift combined with strong, dramatically changing magnetic anomalies (some changes >150 nT; figure 8), strongly support steeply-dipping, sharply-bounded slices of non-magnetic (or reverse polarity) Crescent Formation within the larger magnetic unit.

5.2 Seattle basin

Detailed mapping and geophysical modeling of cross-sections in the Monroe Sultan, and Lake Chaplin geologic quadrangles (Dragovich et al., 2011a, 2013, 2014) constrain the eastern end of the model line that crosses the Seattle basin (B-B' in figures 3-5). This prior work confirms WMB basement containing metagabbro bodies near or at the surface, therefore the eastern end of model B-B' is a simplified version of that work (figure 9). We model the high amplitude, broad magnetic high on the eastern end of the line (MP in figure 4) with buried volcanic rocks, including basalts, within the Eocene-age Seattle basin fill, correlating with Eocene volcanic rocks of Mt. Persis (Dragovich et al, 2011a). The pseudogravity anomaly supports this interpretation, indicating a shallow source, discussed above. The basalts of the volcanic rocks of Mount Persis are arc-related with an adakitic composition that were deposited distal to the volcanic centers (Dragovich et al., 2016; MacDonald et al., 2013) which integrates well with our modeling as a partial basin fill. Tomographic data also support this interpretation (Van Wagoner et al., 2002), which shows a high seismic velocity region where we model the basalts, as well as distinctive offsets on the velocity contours outlining the basement/sediment contact, approximately matching our modeled geometries for the neotectonic offsets across this rock package.

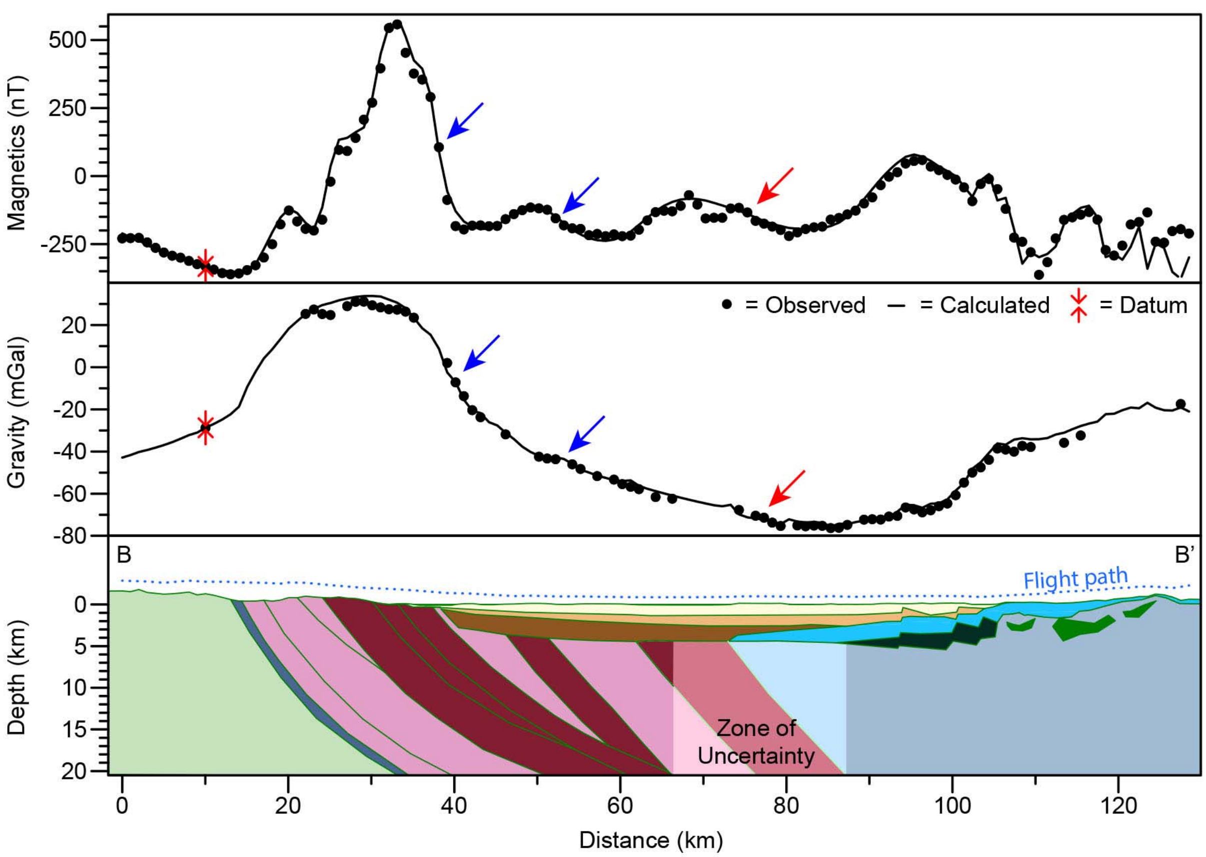

Figure 9

Figure 9. Best-fit model for the Seattle basin. Description and notations described in figure 8. Red arrows show the position of the gradients interpreted as defining Siletzia's eastern edge

(SEB), and blue arrows highlight other candidate gradients discussed in the text, also shown in map view in figure 4.

Active and passive seismic data for the region constrains Seattle basin geometry, depth and stratigraphy in the center of model line B-B' (Johnson et al., 1994; Snelson, 2001; Snelson et al., 2007; ten Brink et al., 2002; Van Wagoner et al., 2002). However, structural details of the basement that affect the gravity and magnetic gradients over the center of the Seattle basin are muted by their depth below the surface (see Supporting Information figure S1). Spatially-correlated but low-amplitude gradients in the magnetic and gravity data (red arrows in figure 9) do support the modeled position of the SEB. However, other spatially-correlated gradients (for example, the blue arrows in figure 9) could be possible boundaries. Modeling experimentation supports the easternmost maximum gradient as the SEB position (figures 4 and 5, gradient #3), coincident with the red arrows in figure 9 and the red star in figure 4. In particular, moving the SEB westward creates predicted gravity and aeromagnetic anomalies over the western half of the Seattle basin that are much lower than the data (see Supporting Information S5). Because the gradients themselves are so low amplitude, our models cannot distinguish between an eastward or westward dip on the SEB (indicated by the "zone of uncertainty" in figure 9; Supporting Information figure S6). Some subtle, small amplitude variations within the magnetic data support dipping slices of non-magnetic (or reverse polarity) Crescent Formation underlying the Seattle basin. Unlike the Seattle uplift line A-A', several geometries of these slices fit the magnetic data equally well along B-B'.

5.3 Kingston arch

The model that crosses the Kingston arch and Everett basin (line C-C' in figures 3-5) has fewer constraints; e.g. wide-angle seismic data are not available along the entire line (Brocher et al., 1999). On the other hand, the simplicity of the model needed to fit the data is encouraging (figure 10). The line is well-constrained by outcrop information on each end of the line, in the west near Port Ludlow and the Olympic Mountains (Dragovich et al., 2002) and to the east within the Lake Chaplin area (Dragovich et al., 2014). Like model B-B', exposures of WMB rocks at the east end of the profile constrain the lithology (Dragovich et al., 2014), and metagabbro bodies of the WMB crop out in this area. The small, Eocene-filled basin (EO in figure 3) is consistent with geologic mapping (Dragovich et al., 2002), but its depth is not well-determined. The depth of the Everett basin (EB in figure 3) and the density of basin fill also are not well constrained. We modeled the fill stratigraphy after the Seattle basin, reasoning that similar regional sediment sources and compaction with depth should yield similar densities.

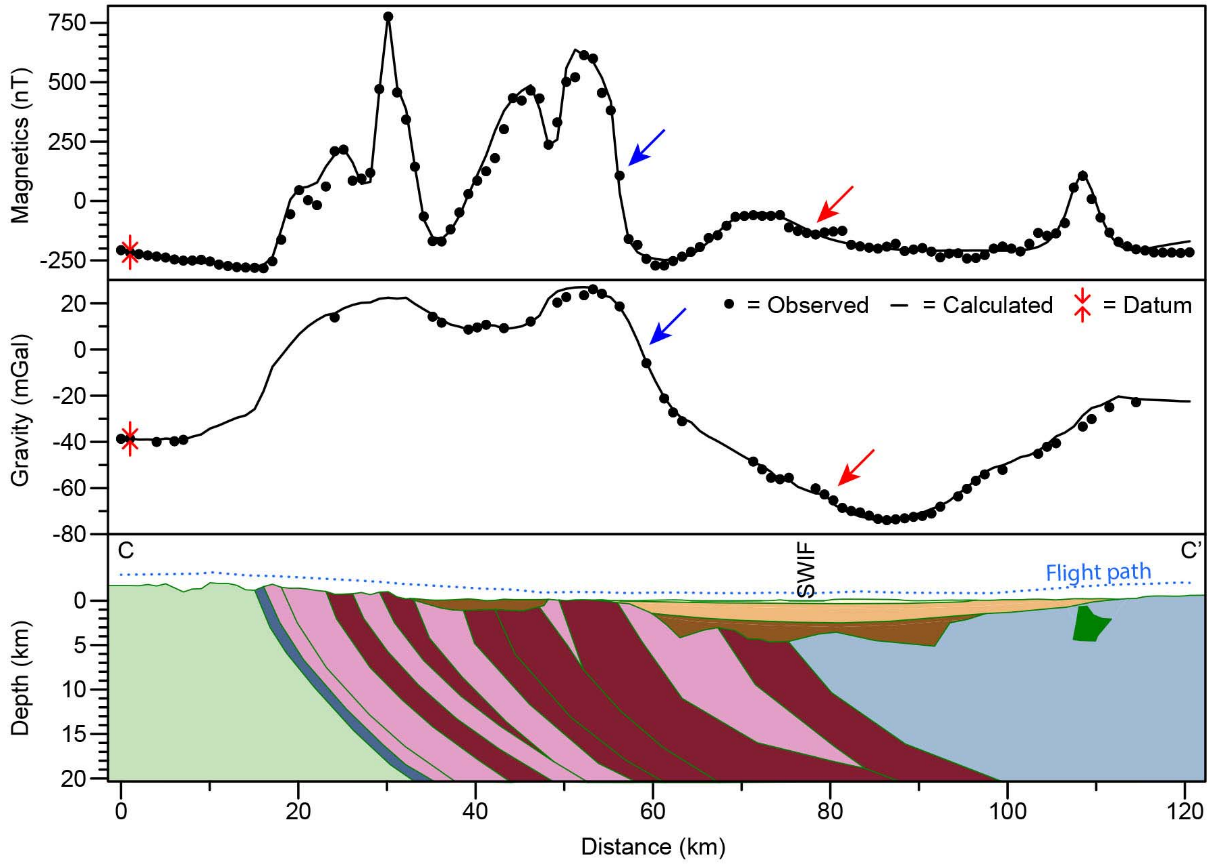

Figure 10

Figure 10. Best-fit model for te Kingston arch. Description and notations described in figure 8. Red arrows show the position of the gradients interpreted as defining Siletzia's eastern edge (SEB), and blue arrows highlight other candidate gradients discussed in the text, also shown in map view in figure 4. SWIF = surface position of the Southern Whidbey Island fault.

Small gravity and magnetic gradients coincide over the Everett basin on Whidbey Island (red arrows on figure 10, red star along gradient #3 in figure 4), but stronger gravity and magnetic gradients also coincide closer to Port Gamble (blue arrows on figure 10, blue star and gradient #1 in figure 4). We modeled both locations and found that placing the SEB near Port Gamble creates an aeromagnetic anomaly that is too low over the western portion of the Everett basin (Supporting Information figure S7). Therefore, we favor gradient #3 on this transect as the boundary, which spatially coincides with the SWIF. The shape of magnetic gradient #3 is most consistent with an eastward dipping boundary (see Supporting Information figure S8 for westward-dipping model). Similar to model A-A', a wide section of this model exhibits Crescent Formation at or quite close to the surface, and the combination of consistently high gravity with strong magnetic gradients suggests fundamental magnetic contrasts within the Crescent Formation, with steeply dipping, sharp boundaries. Therefore, this model also supports systematic, deeply-seated internal structure, within Siletzia. Below we develop a hypothesis that this structure, consistent across our models, is a preserved fold and thrust belt formed during Siletzia accretion.

6 Discussion

6.1 Comparison to other estimations of Siletzia boundary position

Our preferred interpretation is that the SEB trends northward, east of Seattle and through Lake Washington, connects with the SWIF at Possession Sound, and continues northward along the SWIF following the eastern-most gradient in the pseudogravity map (gradient #3 in figures 3-5). This geographic location of the SEB compares favorably to some past estimates. Johnson (1984) placed the boundary just west of Seattle, based in part on stratigraphic observations of Eocene-age sediment. Finn (1990) more quantitatively mapped the boundary from gravity and magnetic anomalies from the greater Oregon/Washington margin. She identified co-located linear gradients in aeromagnetic and gravity anomalies near longitude 123ºW and south of latitude 47ºN, and included the SEB in a 2-D model based on magnetic and Bouguer gravity anomalies south of our study area. Our location for the SEB in model A-A' agrees precisely with Finn's (1990) interpretation. To the north, however, she traced the boundary westward along the Seattle fault, approximately along gradient #1 (figures 3-5). Finn noted low-density "Cascade crust" east of the SEB, which she interpreted as an accretionary prism, similar to our WMB. Based on these comparisons, it is likely the trends identified in the Puget Lowland continue southward.

Snelson et al. (2001, 2007) used active seismic tomography and Bouguer gravity anomalies along an east-trending line through the Seattle basin to interpret the position of the SEB. In particular, tomographic images show lower seismic velocities (~5.7 km/s at 10 km depth) for basement under the eastern half of the Seattle basin as opposed to the west (~6.4 km/s); the transition occurs across a 10-km wide zone. Based on 2-D models of Bouguer gravity, Snelson (2001) favored an SEB 5 km west of our location, which is within the zone of transition for basement velocities in the tomography.

Passive seismic tomographic studies (Calvert et al., 2011; Merrill et al., 2020; Parsons et al., 1999; Ramachandran et al., 2006; Van Wagoner et al., 2002) constraining the SEB location in the mid-crust largely agree with Snelson et al.'s results within the resolution possible with tomographic data. In the 10-20 km depth range in all these models, Crescent Formation rocks have a P-wave approximately 6.5-6.8 km/s and average 6.7 km/s, as expected for metamorphosed basalts at this depth (Christensen and Mooney, 1995; Parsons et al., 1999). Merrill et al. (2020) additionally determined that rocks occupied by the Crescent Formation have high Poisson's ratio (> 0.26) compared to other rocks such as accreted mélange (<0.24). WMB Vp in these models has greater variability than Crescent Formation and ranges from 5.0-6.8 km/s, with an average of 6.1 km/s. We expect variability and lower wave speeds given the low-grade metasedimentary rock types present within the WMB. Poisson's ratio east of the SEB in Merrill's (2020) tomography is just under 0.23, appropriate for mélange. These tomographic studies resolve lateral boundaries to within ~10 km (Parsons et al., 1999; Van Wagoner et al., 2002), about the width of our modeled dipping boundaries, thus the tomographic data may not be able to resolve the dip of the SEB. We do note striking consistencies, however. Parsons et al. (1999) showed two profiles: C, located close to our line A-A', and D, through the east-trending axis of the Seattle basin. On profile C, they interpreted the SEB with slight westward dip, positioned precisely as we have modeled in line A-A'. On profile D, they show an eastward dip as also indicated by our modeling. Calvert et al. (2011) and Ramachandran et al. (2006) show eastward dips of the SEB along our profile C-C', with Ramachandran's study closely matching our modeled boundary in both location and dip.

6.2 Tectonic interpretations of crustal structure

The steep westward dip of the SEB across the Seattle uplift (figure 8), with younger rocks in the hanging wall, is surprising given this is a long-lived eastward-dipping subduction zone. Gravity and magnetic gradients indicate the dip is steep (~60º) and the contact abrupt. The dip of the SEB is compatible with extensional margin models for the formation of Siletzia, and could represent the edge of a rift basin. However, margin rifting predicts interfingering of basalt with sedimentsshed from the continental margin, which is not compatible with the sharpness of the contact as expressed in potential-field data. On the other hand, the westward dip and sharpness of the contact is compatible with obduction of Siletzia eastward onto the North American margin. An obduction interpretation is consistent with the unconformity between the Crescent Formation and overlying Eocene Aldwell Formation, with 3-4 Myr of missing section (Wells et al., 2014; Wells and Coe, 1985), because obduction would cause surface uplift. Structural models for the southeastern boundary of Siletzia in Oregon also suggest a partial obduction or "wedging" mechanism for accretion near Roseburg (Wells et al., 2014; Wells et al., 2000). In this model, Siletz terrane rocks are thrust both over accretionary complex materials (Dothan complex) at deeper levels, and under similar rocks at shallower levels, creating passive roof duplex of Siletz rocks in the upper crust. The structure in the Puget Lowland could be similar, with the obductive part of the boundary closer to the surface.

Modeling across the Kingston arch (model C-C') requires the SEB to dip eastward, opposite in sense to model A-A'. This dip is not surprising because wide-angle seismic reflection studies just to the north across Vancouver Island (Clowes et al., 1987; Hyndman, 1995) clearly show Siletzia and its eastern boundary dipping eastward. The eastward dip for the SEB under Kingston arch does not fit well with the extensional model for the formation of Siletzia. It would require a special explanation for why many Eocene basalts in this region extend for 10's of kilometers under the older, Jurassic-Cretaceous WMB.

Subduction to the north and obduction to the south are consistent with the highest facies of metamorphism observed within Siletzia mafic rocks indicating relative depth of burial (McCrory and Wilson, 2013). Low grade zeolite in the Siletz River Volcanics indicates shallow burial (Wells et al., 2014; figure 1). This transitions to dominantly phrenite-pumpellyite facies in the Olympics with local greenschist (Glassley, 1974; Warnock et al., 1993; Hirsch and Babcock, 2009) and finally to greenschist and amphibolite facies on Vancouver Island (Timpa et al., 2005) indicating progressively deeper burial to the north.

We must explain why and how Cascadia switched from subducting Crescent Formation along the Kingston arch and northward to obducting Crescent Formation along the Seattle uplift and southward. Structural interpretation of the interior of Siletzia under the Puget Lowland may give us a clue. Within our modeled regions of the Siletzia in the Puget Lowland, prominent magnetic highs and lows do not systematically match strong variations in gravity, as would be expected if they were caused by topography on the basement/overlying sediment interface. Forward modeling these magnetic anomalies requires deeply-seated (extending at least to the mid-crust), steeply-dipping panels of Crescent formation with sharply contrasting magnetic properties. Our models include panels of less-magnetic Crescent Formation within an otherwise magnetic terrane, which we interpret as a series of thrust sheets (figure 8). Alternative explanations are 1) the thrust sheet panels responsible for the aeromagnetic lows may have a strong component of reversed remanent magnetization and/or 2) the panels are intrusions with either relatively low or reversed magnetization.

The possibility of reversed remanent magnetization playing some role in creating the aeromagnetic lows observed across the Puget Lowland can't be ignored, as shown by Hagstrum et al. (2002). However, the relationship between reversed basalt and aeromagnetic lows in the Pacific Northwest is not always straightforward. Low aeromagnetic anomalies coincide with the reversed subaerial Eocene Tillamook Volcanics in Oregon, but reversed polarity pillow basalt of the Siletz River Volcanics at Roseburg, Oregon produce strong positive aeromagnetic anomalies (Wells et al., 2014; U.S. Geological Survey, 1996), presumably the result of large viscous component acquired in the present field (Wells et al., 2000). Siletzia's pillow basalt typically has a substantial normal overprint that masks a reversed remanence (e.g. Wells and Coe, 1985).

The panels of Crescent Formation with contrasting magnetization could also represent differently-magnetized intrusions into the Crescent Formation within the mid-shallow crust instead of thrust sheets. A mid-Eocene dike/sill complex is widespread in Oregon (Wells et al., 2014) and dikes are exposed at Gold and Green mountains (Tabor et al., 2011) in the Puget Lowland. The gabbro intrusions at Green and Gold Mountains, are dated at 50.5 Ma (Haeussler and Clark, 2000; Wells et al., 2014), but these intrusions do not spatially coincide with an aeromagnetic anomaly low. In addition, the maximum observed sill/dike thickness in the Tillamook area is just over 2 km, whereas observed aeromagnetic anomalies in our area require variably magnetized panels at least 2 km and more typically 4 km thick or more. Given the thickness of the modeled panels, the fact that we have no direct paleomagnetic observations of the rocks under the Puget Lowland, observed normal overprint of the lower Crescent, and the systematic chemical alteration differences between the upper- and lower members of the Crescent Formation (Babcock et al., 1992) discussed above, we prefer to apply the observed straightforward relationship between overall low susceptibility lower- and high susceptibility upper-member Crescent Formation exposed on the Olympic Peninsula to the rest of our modeling space, which implies thrust-sheet duplication.

Our interpretation of multiple steeply-dipping panels of Crescent formation with contrasting magnetic properties as folded, thrusted, and subsequently eroded Crescent Formation strata above a major decollement (figure 8, bottom panel) implies strong duplication of the Crescent Formation beneath the Puget Lowland during accretion with the North American continent. Model A-A' across the Seattle uplift implies five thrust sheets beyond the eastern edge of the Olympic Mountains with the thickest sheet being ~14 km and a total duplex thickness of ~50 km. The modeled geometries could support shortening on the order of ~50%. This degree of structural deformation has been observed in the Puget Lowland and elsewhere within Siletzia. Babcock et al. (1992) noted the potential for small-scale duplication within the Crescent Formation. Tabor and Cady (1978b) described folding within the Crescent on the east side of the Olympic Peninsula. Wells and Coe (1985) document fault-bounded antiforms in southwestern Washington. Snavely et al. (1993) described faulting and folding in Siletz River Volcanics of the Oregon Coast Range prior to rapid downwarping and deposition of overlying, much less deformed Tyee Formation, and broad folding and local faulting and fracturing of the Siletz River Volcanics was confirmed by Wells et al. (2014). Wells et al. (2000, 2014) mapped a similarly large-scale fold and thrust belt in Siletz River Volcanics near Roseburg, Oregon, which contains basalts tightly folded into anticlinal uplifts, bounded by steeply-dipping reverse faults (40-70°; Wells et al., 2000).

6.3 A terrane accretion hypothesis

We suggest the westward dip of the SEB along line A-A', its flip to an eastward dip along line C-C', and the steeply-dipping wedges of less magnetic rock within the Seattle uplift arose from fold-and-thrust processes at the northern edge of the Siletzia accretionary province.. This agrees most closely with the hypothesis that Siletzia originated as an accreted ocean island chain (Duncan, 1982). Based on our interpretation of the steeply-dipping wedges of less magnetic rock within the Crescent Formation as eastward-dipping thrust sheets, we interpret many linear magnetic gradients coincident with gravity highs across the Puget Lowland as reverse fault contacts. We apply this idea using the pseudogravity gradients identified from figure 5 to extend these hypothesized faults across the Puget Lowland (figure 11) revealing a fold-thrust belt. We lose resolution over the Seattle basin, and do not extend our interpretation to the extreme NW and SW parts of the study area due to lack of modeling support. Our interpretation outlines regional structures only; many smaller scale structures could be involved (as suggested by Babcock et al., 1992) that our analysis does not identify.

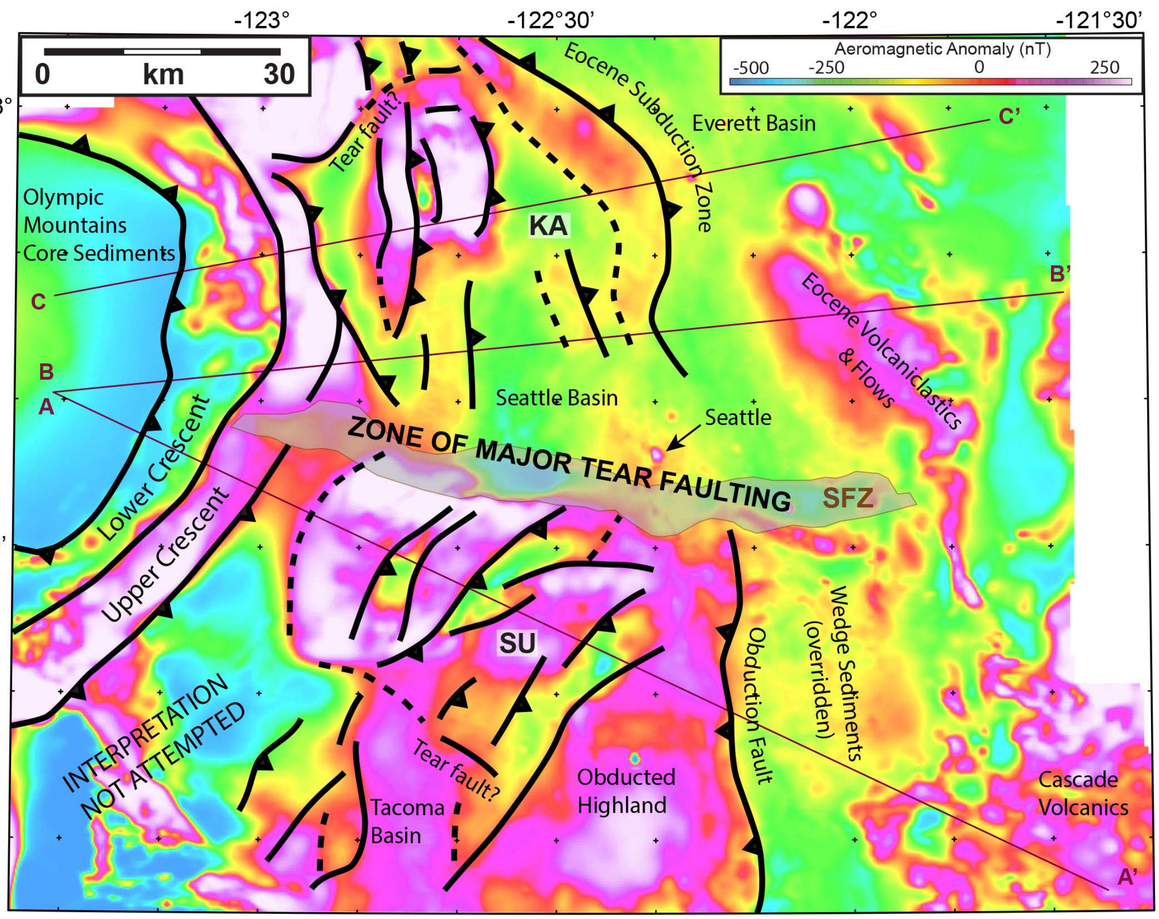

Figure 11

Figure 11. Fold and thrust belt interpretation superimposed on the aeromagnetic map. Interpreted reverse faults bear hachures. Unadorned, solid lines show the positions of other boundaries, many of which we interpret as the boundary between the upper and lower Crescent formations, especially where they are positioned parallel to and between two reverse faults. All lines closely follow linear maximum gradients identified from the pseudogravity map (figure 5), however, dotted lines indicate linear features that are less certain. Solid boundaries and reverse faults in the Olympic Mountains (bordering the area marked as mapped upper and lower Crescent) also have geologic mapping support. Labels identify major tectonic elements corresponding to the text and the light brown lines indicate the positions of the geophysical models in figures 8-10. KA = Kingston arch; SFZ (grey area) = Seattle fault zone; SU = Seattle uplift.

Given large post-Eocene rotation of Siletzia mafic rocks in Oregon (up to 75 degrees clockwise rotation) and southwest Washington (e.g. Globerman et al., 1982; Simpson and Cox, 1977; Wells et al., 2014; Wells and Coe, 1985; Wells and Heller, 1988), we must consider the possibility that today's interpreted fault orientations have rotated since the Eocene. However, paleomagnetic studies of the Olympic Mountains and exposures in the Puget Lowland have mean paleomagnetic directions nearly identical to the expected Eocene direction (Beck and Engebretson, 1982; Warnock et al., 1993), including rocks both on the Seattle uplift (along A-

A') and the Kingston Arch (nearer to C-C'). This indicates that these structures have not rotated much, if at all since the Eocene.

This map-view interpretation (figure 11) highlights a structural transition between the Seattle uplift and Kingston arch, in addition to the change in dip of the SEB. The linear and parallel trend of the pseudogravity gradients lends credence to the fault-interpretation idea and shows two distinctive orientations: NE trending over the Seattle uplift and Tacoma basin and NNW trending over the Seattle basin and Kingston arch. The transition between these two zones occurs over a rather short length-scale (~10 km or less). We suggest that the transition consists of an E-trending tear fault at the approximate current latitude of the Seattle fault. Tectonically, there could be other reasons for such a transition in fold and thrust belt morphology, such as development of a lateral ramp or spatial requirements imposed by a change in geometry of the subducting plate. However, a tear fault must accommodate some portion of this transition due to the change in in dip on the SEB fault.

Why would the structural trends be different in the north and south? Recent crustal-scale seismic tomography images computed from USArray data (Gao et al., 2011; Schmandt and Humphreys, 2011) suggest that an embayment existed in the Eocene subduction zone, coinciding spatially with the SWIF at the northern end of our study area, with slow crustal velocities extending north and east attributed to accretionary wedge sediments. These studies interpret an accretionary model for the amalgamation of Siletzia with North America, with Siletzia being a volcanic plateau rafted in on the subducting plate (Trehu et al., 1994). The SWIF is interpreted as the subducted edge of the Crescent Formation in the northern part of the Puget Lowland. We interpret the interleaved slivers of variably magnetized Crescent basalt west of the SWIF as a fold and thrust belt striking subparallel to the trench axis that consists of thrust sheets detached from the subducting plate and accreted to the Cretaceous-Eocene wedge (figure 12a). The terrane boundary transitions into a generally NE-dipping SEB on central Vancouver Island, where Siletzia is only 10 km thick (Clowes et al. 1987; Hyndman, 1995). Magnetic anomalies observed over Vancouver Island show a single, simple magnetic high over the Crescent Formation (Dehler and Clowes, 1992; Hyndman, 1995) consistent with a thinner slice, unlike our observed, more complex magnetic anomalies over the Puget Lowland.

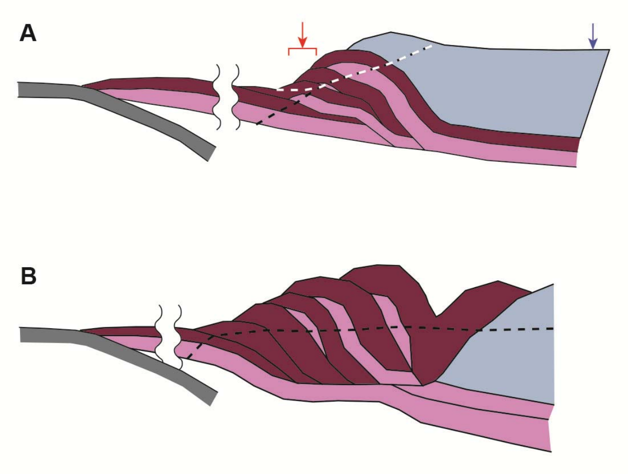

Figure 12

Figure 12. Tectonic cartoon of the structure of the fold and thrust belt along the a) Kingston arch profile (figure 10) and b) Seattle uplift profile (figure 8) in the early Eocene, after accretion of Siletzia. Grey slab shows the newly subducting slab, with the break indicating uncertainty of relative placement of the newly-formed subduction zone and the fold and thrust belt. Maroon blocks are upper Crescent, and pink is lower Crescent. Western mélange belt (WMB) is blue. The black, dotted line shows current erosional level. White dotted line in (a) shows inferred erosional level in the Eocene at the end of the period of accretion. The red arrow shows the potential location of deposition of the Aldwell formation. The blue arrow shows the approximate location of paleoflow direction reversals within the Swauk formation from Eddy et al. (2015). Slices of lower Crescent beneath the WMB in (b) results from delamination of upper and lower Crescent during accretion (corresponding upper layers are preserved in the fold and thrust belt) and subduction of the lower Crescent along with the downgoing slab mantle.

In contrast, line A-A' indicates obduction of Siletzia onto the North American continent, implying resistance to subduction. Thick oceanic plates likely resist subduction (e.g. Gans et al., 2011; Gutscher et al., 2000), and oceanic plateaus tend to stall subduction and become accreted to the overriding plate, an excellent example being the Ontong Java plateau (Petterson et al., 1997). This is consistent with thickening of Siletzia southward (Trehu et al., 1994); seismic and geologic map data support an estimated thickness of thicknesses of ~16 km for Crescent Formation in the Olympic Mountains (Babcock et al., 1992; Tabor and Cady, 1978a), much thicker than on Vancouver Island, and even thicker in Oregon (33-35 km; Fleming and Trehu, 1999; Trehu et al., 1994). A thicker original Siletzia crust at the latitude of A-A' is consistent with our modeling, which contains a greater proportion and thicker slices of what we interpret to be upper Crescent Formation, as compared to C-C' (figure 12). Any sort of consideration of structural balancing within the development of a fold and thrust belt of this geometry (e.g. figure 12b) requires subduction of substantial lengths of the lower crust eastward under the WMB, present Cascadia arc, and perhaps even farther. Recent interpretations of regional crustal wave velocities from ambient noise tomography under the arc and eastward suggest high velocity regions in the lower crust, consistent with thick basalt (Gao et al., 2011). Conversely, the lower crust could have subducted with the mantle of the down-going plate.

If resistance to subduction is related to plateau thickness, then we expect south-to-north variation in local stress orientations during accretion-related thrust faulting following obduction of the plateau. This would promote rotation of the shortening direction from west to northwest, wrapping around the edge of the thicker, obducted segment (figure 13), as observed for salients within modern fold and thrust belts with indentors. Analog experimental studies show that stress trajectories fan in advance of the indentor due to differential shortening along the length of the margin (e.g. Marshak, 2004; Molnar and Tapponnier, 1975; Reiter et al., 2011), thus thrust wedges curve to mimic the shape of the indentor. In the case of the Puget Lowland, the indentor would be the thick center of the obducted plateau, already accreted to the continent, and the indented material the trailing, thinner northwest edge of the plateau (figure 13), which continues to move east and accrete after obduction/docking of the plateau. The edge of the salient paralleling the transport direction is transpressive (Marshak, 2004), thus tear faults are common at the edge of such indentors, especially if the indentor has a relatively abrupt edge. Due to its position on the edge of the salient and its orientation parallel to the overall transport direction, the Seattle fault could have originated as an oblique slip tear fault during obduction in the Eocene (figure 13) and was later rejuvenated as a reverse fault due to regional north-south compression.

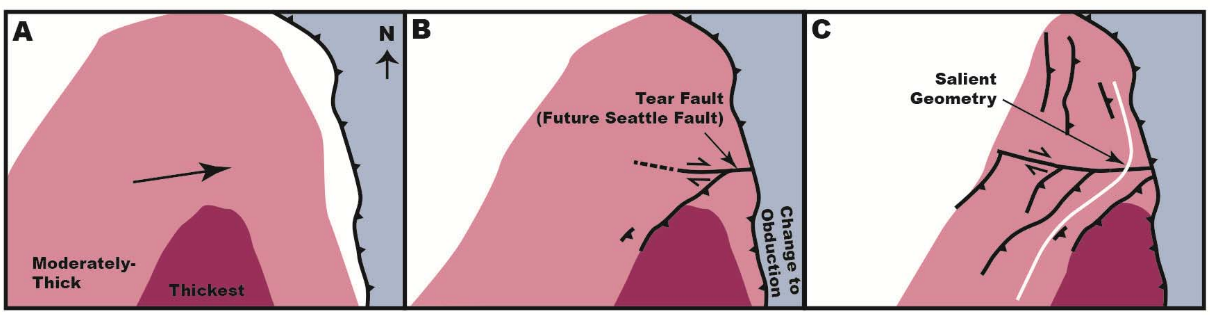

Figure 13

Figure 13. Model for the development of the Siletzia fold and thrust belt. Colors indicate relative thickness of Siletzia crust on the subducting plate. Large arrow indicates general eastward movement of the subducting plate relative to overriding plate. a) Generalized geometry just prior to subduction of Siletzia. b) As the thickest part of Siletzia meets the subduction zone, it resists, and the subductive boundary changes to obductive. As the thickest part of Siletzia slows down, thrust faults develop to the west. A tear fault develops to accommodate the difference in shortening from north to south. c) As subuction and obduction continues, the tear fault accommodates both a difference in shortening and fault orientation between north and south. In the north, faults parallel the subduction zone, and in the south, faults parallel the edge of the thickest part of Siletzia, now stuck to the edge of the North American continent.

6.4 Implications of terrane accretion for the sedimentary record

A fold and thrust belt within the Crescent Formation under the Puget Lowland should be consistent with the structure and stratigraphy of overlying early to mid-Eocene sedimentary units. Examining these records could be a fruitful way to test the details of our hypothesis. Thorough examination of the evidence is beyond the scope of this paper, but we point to a couple of pieces of evidence already studied that may support our hypothesis. Possibly the most useful unit to examine is the marine mid-Eocene Aldwell Formation (Squires et al., 1992). A regional unconformity at the base of the Aldwell and missing section beneath the unconformity (Tabor and Cady, 1978a, 1978b; Wells et al., 2014) is consistent with regional uplift and erosion during Crescent Formation accretion. These marine sedimentary rocks east and north of the Olympic Mountains include a basal boulder conglomerate up to 30 m thick composed of locally-derived Crescent Formation clasts (Squires et al., 1992). Uplifted and eroded highlands produced by a fold and thrust belt within the Crescent south and east of this area would be a plausible source. Our schematic cross section of the Crescent fold and thrust belt predicts the Aldwell in this location would have been deposited in a forearc basin (see red arrow in figure 12a).

More recently Eddy et al. (2015) have documented the timing of sedimentation and deformation of Paleogene continental sequences in the North Cascades with extensive U/Pb ages on magmatic and detrital zircons. They demonstrate that paleoflow reversals within these units (blue arrow marks the approximate location in figure 12a) followed by unconformity development and compressional deformation between 51.3 and 49.9 Ma is consistent with the development of a highland within or adjacent to accreted Siletzia during this time.

6.5 Neotectonic implications of crustal structure

Our tectonic model requires a tear fault at the current location of the Seattle fault. Previously, the Seattle fault has been interpreted as a rather steeply-dipping structure at depth (Brocher et al., 2004; Pratt et al., 1997; ten Brink et al., 2002); could the steep dip and location of the Seattle fault have been influenced by what was probably a steeply-dipping zone of tear faulting? This type of prior crustal deformational history could affect our interpretation of total offset on more recently-active faults. If the area of Siletzia south of the Seattle fault was an obducted fold and thrust belt, it may have been elevated in the Eocene higher than the subducted fold and thrust belt to the north. If such an elevation difference persisted, it would contribute to current estimates of total throw on the Seattle fault.

Other than the Seattle fault and the northernmost SWIF within our study area, here is a notable lack of clearly identified neotectonic faults with major offset coincident with the structures we model. As noted above, most neotectonic faults in the region coincide with pseudogravity and isostatic gradients that are weaker than the Siletzia-related boundaries we model (SWIF, and RF on figures 3 and 5). Thus, it is unlikely that these structures accommodate significant (i.e. extending into the mid-crust) vertical offset, nor do they juxtapose Crescent Formation against WMB. The SWIF clearly trends southeast and likely merges with more S-trending faults such as the Rattlesnake Mountain fault zone well east of the SEB (figures 4 and 5) near Monroe (Allen et al., 2017; Dragovich et al., 2011a). Indeed, the eastern portion of the Puget Lowland from North Bend to Monroe contains multiple strike-slip fault strands trending NNE and NNW (Allen et al., 2017; Dragovich et al., 2008, 2010b, 2011a). This relationship suggests that crust of predominantly WMB lithology is easier to deform than the Crescent Formation, and the neotectonic faults are preferentially breaking through this unit. Data tracking plate motion (such as GPS) suggests that Siletzia is a fairly strong, coherent block largely translating northward in the forearc of Cascadia (Magill et al., 1982; McCaffrey et al., 2007; Wells and McCaffrey, 2013; Wells et al., 1998). There are places within the interior of Siletzia where neotectonic faults are active. However, for places in close proximity to the SEB, deformation may focus within the weaker WMB rock package rather than along its boundary with Siletzia. Merrill (2020) corroborates this idea, showing a correlation of small magnitude seismicity within crust that has Poisson's ratio below 0.24 (whereas Siletzia has a Poisson's ratio of 0.26). He particularly shows seismicity clustering in the mid-upper crust east of the SEB in his model (within our interpreted WMB), not along the SEB itself. We also note that the mid-crustal decollement required for our fold and thrust belt model for accretion also fits well with seismicity patterns. The Puget Lowlands are underlain by a mid-crustal band of consistent modern seismicity (Hyndman et al., 2003). Merrill et al. (2020) relocated this seismicity which showed that much of it under the greater Seattle region is below the region they interpret as Siletzia, which they suggest could be due to impermeability of Siletzia to infiltrating fluids. They prefer the interpretation that the more permeable materials occupying the lower crust are either underplated North American rocks (as would be expected with obduction of the upper crust) or underplated mafic and felsic rocks from subsequent subduction.

The change in basement type beneath basins will affect models of basin shape inferred from regional gravity anomalies (Brocher et al., 2001) if they are used for the purpose of modeling ground motion during major earthquakes (Frankel and Stephenson, 2000; Pratt et al., 2003; Wirth et al., 2019). A lower density, lower velocity crust (i.e., the WMB) under the eastern portion of the Seattle basin as opposed to Crescent Formation would result in a shallower modeled basement depth and a smaller velocity contrast across the sediment/basement boundary. As noted above, gradients #2 and 3 coincide with a transition in the character of a low gravity anomaly, with the western part of the Seattle basin appearing shallower, with a less pronounced gravity low than the eastern part of the basin (figure 3). Though past inversions and interpretations from seismic data have shown a rather symmetrical Seattle basin east to west (Brocher et al., 2001), site response analysis of major earthquakes shows a greater response east of Lake Washington, as for teleseismic waves measured from the Chi Chi earthquake shown by Pratt et al. (2003). They interpret the greater amplification as most likely due to focusing and convergence of seismic waves, as would be expected if the Seattle basin were shallower to the east, opposite that suggested by a simpler interpretation of the gravity without underlying basement contrasts. Thus, a full understanding of major crustal components and structures such as given by this study will support more robust and detailed hypotheses about how seismic wave amplification will vary across the region during future large magnitude earthquakes, why modern seismicity is clustered heterogeneously throughout the Puget Lowland, and where earthquakes are more likely to happen in the future.

7 Conclusions

We have mapped and modeled the internal structure and eastern boundary of Siletzia in the Puget Lowland of Washington State utilizing gravity, magnetic, and seismic data. The eastern boundary of Siletzia abuts the western mélange belt, trends northward through Lake Washington to merge with the Southern Whidbey Island fault at Possession Sound. We definitively show that in the mid-upper crust, Siletzia does not extend east of the latitude of Lake Washington. We use these models to estimate the dip of Siletzia's eastern boundary at several positions along its length, revealing a westward-dipping Siletzia contact where it crosses the Seattle uplift in the south, and an eastward-dipping contact across the Kingston arch to the north. Our model also includes steeply-dipping, deeply-rooted slices of non-magnetic Crescent basement beneath the Puget Lowland, consistent with fold-and-thrust deformation of the mid-upper crustal Crescent Formation during accretion of Siletzia with North America. Based on the transition in orientation, structural style, and crustal thickness from north to south across the Puget Lowland, we arguefor an obducted highland in the south and a subducted geometry to the north. This narrow north-south transition was potentially accommodated by an east-west tear fault located approximately at the latitude of the modern Seattle fault, implying a pre-Oligocene history for this still-active fault. Our interpreted crustal structure provides a basis on which to superimpose effects of modern tectonic processes. The spatial distribution we define for lithologic rheologies likely affect modern fault kinematics and dynamics important for seismic hazard determination. These lithologic distributions also provide new constraints for more accurate determinations of the shape of Puget Lowland basins for ground motion characterization.

Acknowledgments

Funding and material support was provided by USGS Mendenhall Postdoctoral Program, the Colorado College (CC) Natural Sciences Division and CC Geology Department Getty Fund. This project used detailed mapping supported by the Washington Geological Survey and USGS STATEMAP grant program. We thank Tom Pratt, Tom Brocher, Brian Sherrod, Sam Johnson, and Ralph Haugerud for thoughtful guidance on Puget Lowland structure and history. CC students Meredith Bush, and Wiley Skewes, and Sarah Geisse assisted in the field and provided confirmation of ideas with their associated modeling efforts. Bob Morin and Vicki Langenheim, USGS, provided data, and David Ponce, Donald Plouff, Dan Scheirer and Bruce Chuchel provided software support. Thanks to Nikolas Midttun for substantive manuscript feedback.

Open Research

Gravity data used for mapping and analysis that are not cited in text are included in Table S1 of the Supporting Information for review purposes. They will be posted on the Washington Geological survey Geologic Information Portal (https://www.dnr.wa.gov/geologyportal) for free public download upon publication. Hand sample/outcrop physical property measurements used as a basis for developing model physical properties are included for review in Table S2 of the Supporting Information. These data will be made publically available online at the Washington Geological Survey with a download link upon publication. Oasis Montaj (Geosoft, 2016) used for potential fields data gridding and filtering as well as forward model construction is available via subscription from Geosoft, Inc.

References

Anderson, M. L., Blakely, R. J., Wells, R. E., & Dragovich, J. (2011). *Eastern boundary of the Siletz terrane in the Puget Lowland from gravity and magnetic modeling with implications for seismic hazard analysis*. Paper presented at AGU Fall Meeting, American Geophysical Union, San Francisco, CA, December 5-9, Abstract GP33B-06.

Allen, M. D., Mavor, S. P., Tepper, J. H., Nesbitt, E. A., Mahan, S. A., Cakir, R., Stoker, B. A., & Anderson, M. L. (2017). *Geologic map of the Maltby 7.5-minute quadrangle, Snohomish and King Counties, Washington* (Map 2017-02, 42 p., 1 sheet, scale 1:24,000). Olympia: Washington State Division of Geology and Earth Resources.

Babcock, R., Burmester, R., Engebretson, D., Warnock, A., & Clark, K. (1992). A rifted margin origin for the Crescent Basalts and related rocks in the northern Coast Range volcanic province, Washington and British-Columbia. *Journal of Geophysical Research-Solid Earth, 97(B5)*, 6799-6821. doi:10.1029/91JB02926

Barnes, D. F., Oliver, H. W., & Robbins, S. L. (1969). Standardization of gravimeter calibrations in the Geological Survey. *Eos Transactions, American Geophysical Union, 50(10)*, 626-627.

Beck, M. E. Jr., & Engebretson, D. C. (1982). Paleomagnetism of small basalt exposures in the West Puget Sound area, Washington, and speculations on the accretionary origin of the Olympic Mountains. *Journal of Geophysical Research, 87*, 3755-3760. doi:10.1029/JB087iB05p03755

Blakely, R. J. (1995). *Potential Theory in Gravity and Magnetic Applications*. Cambridge : Cambridge University Press.

Blakely, R. J., Brocher, T. M., & Wells, R. E. (2005). Subduction-zone magnetic anomalies and implications for hydrated forearc mantle. *Geology, 33(6)*, 445-448. doi:10.1130/G21447.1

Blakely, R. J., Sherrod, B. L., Hughes, J. F., Anderson, M. L., Wells, R. E., & Weaver C. S. (2009). Saddle Mountain fault deformation zone, Olympic Peninsula, Washington: Western boundary of the Seattle uplift. *Geosphere, 5(2)*, 105-125. doi:10.1130/GES00196.1

Blakely, R. J., Wells, R. E., & Weaver, C. S. (1999). *Puget Sound aeromagnetic maps and data* (Open-File Report 99-0514). Reston, VA: U.S. Geological Survey.

Blakely, R. J., Wells, R. E., Weaver, C. S., & Johnson, S. Y. (2002). Location, structure, and seismicity of the Seattle fault zone, Washington: Evidence from aeromagnetic anomalies, geologic mapping, and seismic-reflection data. *Geological Society of America Bulletin, 114(2)*, 169-177. doi:10.1130/0016-7606(2002)1142.0.CO;2

Blakely, R. J., John, D. A., Box, S. E., Berger, B. R., Fleck, R. J., Ashley, R. P., Newport, G. R., & Heinemeyer, G. R. (2007). Crustal controls on magmatic-hydrothermal systems: A geophysical comparison of White River, Washington, with Goldfield, Nevada. *Geosphere, 3(2)*, 91-107. doi:10.1130/GES00071.1

Brocher, T. A. (2005). Empirical relations between elastic wavespeeds and density in the Earth's crust. *Bulletin of the Seismological Society of America, 95(6)*, 2081-2092. doi:10.1785/0120050077

Brocher, T. M., Blakely, R. J., & Wells, R. E. (2004). Interpretation of the Seattle Uplift, Washington, as a passive-roof duplex. *Bulletin of the Seismological Society of America, 94(4)*, 1379-1401.

Brocher, T. M., & Christensen, N. I. (2001). *Density and velocity relationships for digital sonic and density logs from coastal Washington and laboratory measurements of Olympic Peninsula mafic rocks and greywackes* (Open-File Report 01-264). Reston, VA: U.S. Geological Survey.

Brocher, T. M., Parsons, T., Blakely, R. J., Christensen, N. I., Fisher, M. A., Wells, R. E., & SHIPS Working Group (2001). Upper crustal structure in Puget Lowland, Washington: Results from the 1998 Seismic Hazards Investigation in Puget Sound. *Journal of Geophysical Research, 106(B7)*, 13541-13564. doi:10.1029/2001JB000154

Brocher, T. M., Parsons, T., Creager, K. C., Crosson, R. S., Symons, N. P., Spence, G. D., Zelt, B. C., Hammer, P. T. C., Hyndman, R. D., Mosher, D. C., Trehu, A. M., Miller, K. M., ten Brink, U. S., Fisher, M. A., Pratt, T. L., Alvarez, M. G., Beaudoin, B. C., Louden, K. E., & Weaver, C. S. (1999). *Wide-angle seismic recordings from the 1998 Seismic Hazards Investigation of Puget Sound (SHIPS), western Washington and British Columbia* (Open-File Report 99-314). Reston, VA: U.S. Geological Survey.

Brocher, T. M., & Ruebel, A. L. (1998). *Compilation of 29 sonic and density logs from 23 oil test wells in western Washington State* (Open-File Report 98-249). Reston, VA: U.S. Geological Survey.

Calvert, A. J., Preston, L. A., & Farahbod, A. M. (2011). Sedimentary underplating at the Cascadia mantle-wedge corner revealed by seismic imaging. *Nature Geoscience, 4(8)*, 545-548. doi:10.1038/NGEO1195

Christensen, N. I., & Mooney, W. D. (1995). Seismic velocity structure and composition of the continental crust; a global view. *Journal of Geophysical Research, 100*, 9761-9788. doi:10.1029/95JB00259

Clowes, R., Brandon, M., Green, A., Yorath, C., Brown, A., Kanasewich, E., & Spencer, C. (1987). Lithoprobe - Southern Vancouver-Island - Cenozoic subduction complex imaged by deep seismic reflections. *Canadian Journal of Earth Sciences, 24(1)*, 31-51. doi:10.1139/e87-004

Czajkowski, J. L., & Bowman, J. D. (2014). *Faults and earthquakes in Washington State* (Open-File Report 2014-05). Olympia, WA: Washington State Division of Geology and Earth Resources.

Dehler, S. A., & Clowes, R. M. (1992). Integrated geophysical modelling of terranes and other structural features along the western Canadian margin. *Canadian Journal of Earth Sciences, 29(7)*, 1492-1508. doi:10.1139/e92-119

Dragovich, J. D., Anderson, M. L., MacDonald J. H. Jr., Mahan, S. A., DuFrane, S. A., Littke, H. A., Wessel, G. R., Saltonstall, J. H., Koger, C. J., & Cakir, R. (2010a). *Supplement to the geologic map of the Carnation 7.5-minute quadrangle, King County, Washington: Geochronologic, geochemical, point count, geophysical, earthquake, fault, and neotectonic data* (Open File Report 2010-2). Olympia, WA: Washington State Division of Geology and Earth Resources.

Dragovich, J. D., Anderson, M. L., Mahan, S. A., Koger, C. J., Saltonstall, J. H., MacDonald, J. H. Jr., Wessel, G. R., Stoker, B. A., Bethel, J. P., Labadie, J. E., Cakir, R., Bowman, J. D., & DuFrane, S. A. (2011a). *Geologic map of the Monroe 7.5-minute quadrange, King and Snohomish Counties, Washington* (Open-File Report 2011-1). Olympia, WA: Washington State Division of Geology and Earth Resources.

Dragovich, J. D., Anderson, M. L., Mahan, S. A., MacDonald, J. H. Jr., McCabe, C. P., Cakir, R., Stoker, B. A., Villeneuve, N. M., Smith, D. T., & Bethel, J. P. (2012). *Geologic map of the*

Lake Joy 7.5-minute quadrangle, King County, Washington (Map 2012-01, 83 p., 1 plate, scale 1:24,000). Olympia: Washington State Division of Geology and Earth Resources.

Dragovich, J. D., Anderson, M. L., Walsh, T. J., Johnson, B. L., & Adams, T. L. (2007). *Geologic map of the Fall City 7.5-minute quadrangle, King County, Washington* (Map GM-67, 16 p., 1 plate, scale 1:24,000). Olympia: Washington State Division of Geology and Earth Resources.

Dragovich, J. D., Frattali, C. L., Anderson, M. L., Mahan, S. A., MacDonald, J. H. Jr., Stoker, B. A., Smith, D. T., Koger, C. J., Cakir, S. R., DuFrane, A., & Sauer, K. B. (2014). *Geologic map of the Lake Chaplain 7.5-minute quadrange, Snohomish County, Washington* (Map 2014-01, 51 p., 1 plate, scale 1:24,000). Olympia: Washington State Division of Geology and Earth Resources.

Dragovich, J. D., Littke, H. A., Anderson, M. L., Hartog, R., Wessel, G. R., DuFrane, S. A., Walsh, T. J., MacDonald, J. H. Jr., Mangano, J. F., & Cakir, R. (2009). *Geologic map of the Snoqualmie 7.5-minute quadrangle, King County, Washington* (Map GM-75, 2 sheets, scale 1:24,000). Olympia: Washington State Division of Geology and Earth Resources.

Dragovich, J. D., Littke, H. A., Anderson, M. L., Wessel, G. R., Koger, C. J., Saltonstall, J. H., MacDonald, J. H. Jr., Mahan, S. A., & DuFrane, S. A. (2010b). *Geologic map of the Carnation 7.5-minute quadrangle, King County, Washington* (Open File Report 2010-1). Olympia, WA: Washington State Division of Geology and Earth Resources.

Dragovich, J. D., Littke, H. A., Mahan, S. A., Anderson, M. L., MacDonald, J. H. Jr., Cakir, R., Stoker, B. A., Koger, C. J., Bethel, J. P., DuFrane, S. A., Smith, D. T., & Villeneuve, N. M. (2013). *Geologic map of the Sultan 7.5-minute quadrangle, King and Snohomish Counties, Washington* (Map 2013-01, 57 p., 1 plate, scale 1:24,000). Olympia: Washington State Division of Geology and Earth Resources.

Dragovich, J. D., Logan, R. L., Schasse, H. W., Walsh, T. J., Lingley, W. S. J., Norman, D. K., Gerstel, W. J., Lapen, T. J., Schuster, J. E., & Meyers, K. D. (2002). *Geologic map of Washington State - Northwest quadrant* (Map GM-50, scale 1:250,000). Olympia: Washington State Division of Geology and Earth Resources.

Dragovich, J. D., Mahan, S. A., Anderson, M. L., MacDonald, J. H. Jr., Wessel, G. R., DuFrane, S. A., Cakir, R., Bowman, J. D., & Littke, H. A. (2011b). *Analytical data from the Monroe 7.5-minute quadrangle, King and Snohomish Counties, Washington: supplement to Open File Report 2011-1* (Open File Report 2011-2). Olympia, WA: Washington State Division of Geology and Earth Resources.

Dragovich, J. D., Mavor, S. P., Anderson, M. L., Mahan, S. A., MacDonald, J. H. Jr., Tepper, J. H., Smith, D. T., Stoker, B. A., Koger, C. J., Cakir, R., DuFrane, S. A., Scott, S. P., & Justman, B. J. (2016). *Geologic map of the Granite Falls 7.5-minute quadrangle, Snohomish County, Washington* (Map 2016-03, 63 p., 1 sheet, scale 1:24,000). Olympia: Washington State Division of Geology and Earth Resources.

Dragovich, J. D., Walsh, T. J., Anderson, M. L., Hartog, R., DuFrane, S. A., Vervoot, J., Williams, S. A., Cakir, R., Stanton, K. D., Wolff, F. E., & Norman, D. K. (2008). *Geologic map of the North Bend 7.5-minute quadrangle, King County, Washington* (Map GM-73, 39 p., 1 plate, scale 1:24,000). Olympia: Washington State Division of Geology and Earth Resources.

Duncan, R. (1982). A captured island chain in the coast range of Oregon and Washington. *Journal of Geophysical Research, 87(B13)*, 10,827–10,837. doi: 10.1029/JB087iB13p10827

Eddy, M. P., Bowring, S. A., Umhoefer, P. J., Miller, R. B., McLean, N. M., & Donaghy, E. E. (2015). High-resolution temporal and stratigraphic record of Siletzia's accretion and triple junction migration from nonmarine sedimentary basins in central and western Washington. *Geological Society of America Bulletin, 128(3-4)*, 425-441. doi:10.1130/B31335.1

Finn, C. (1990). Geophysical Constraints on Washington Convergent Margin Structure. *Journal of Geophysical Research, 95(B12)*, 19,533-19,546. doi:10.1029/JB095iB12p19533

Finn, C., Phillips, W. M., & Williams, D. L. (1991). *Gravity anomaly and terrain maps of Washington* (Geophysical Investigations Map GP-988, scale 1:500,000 and 1:1,000,000). Reston: U.S. Geological Survey.

Fleming, S., & Trehu, A. (1999). Crustal structure beneath the central Oregon convergent margin from potential-field modeling: Evidence for a buried basement ridge in local contact with a seaward dipping backstop. *Journal of Geophysical Research, 104(B9)*, 20431-20447. doi:10.1029/1999JB900159

Frankel, A., & Stephenson, W. (2000). Three-dimensional simulations of ground motions in the seattle region for earthquakes in the Seattle fault zone. *Bulletin of the Seismological Society of America, 90(5)*, 1251-1267. doi:10.1785/0119990159

Gans, C. R., Beck, S. L., Zandt, G., Gilbert, H., Alvarado, P., Anderson, M., & Linkimer, L. (2011). Continental and oceanic crustal structure of the Pampean flat slab region, western Argentina, using receiver function analysis: New high-resolution results. *Geophysical Journal International, 186(1)*, 45-58. doi:10.1111/j.1365-246X.2011.05023.x

Gao, H., Humphreys, E. D., Yao, H., & van der Hilst, R. D. (2011). Crust and lithosphere structure of the northwestern US with ambient noise tomography: Terrane accretion and Cascade arc development. *Earth and Planetary Science Letters, 304(1-2)*, 202-211. doi:10.1016/j.epsl.2011.01.033

Gardner, G., Gardner, L., & Gregory, A. (1974). Formation velocity and density - Diagnostic basics for stratigraphic traps. *Geophysics, 39(6)*, 770-780. doi:10.1190/1.1440465

Geosoft, Inc. (2014). Oasis Montaj Gridding: A How-To Guide. Geosoft Inc., Toronto. http://updates.geosoft.com/downloads/files/how-to-guides/Oasis_montaj_Gridding.pdf.

Geosoft, Inc. (2016). Oasis Montaj (Ver. 9.0): Data Processing and Analysis Systems for Earth Science Applications [Software]. Geosoft Inc., Toronto.

Glassley, W. (1974). Geochemistry and Tectonics of Crescent Volcanic-Rocks, Olympic peninsula, Washington. *Geological Society of America Bulletin, 85(5)*, 785-794. doi:10.1130/0016-7606(1974)852.0.CO;2

Globerman, B. R., Beck, M. E. Jr., & Duncan, R. A. (1982). Paleomagnetism and tectonic significance of Eocene basalts from the Black Hills, Washington Coast Range. *Geological Society of America Bulletin, 93(11)*, pp.1151-1159.

Groome, W. G., Thorkelson, D. J., Friedman, R. M., Mortensen, J. K., Massey, N. W. D., Marshall, D. D., & Layer, P. W. (2003). Magmatic and tectonic history of the Leech River Complex, Vancouver Island, British Columbia: Evidence for ridge-trench intersection and accretion of the Crescent Terrane. In Sisson, V. B., Roeske, S. M., Pavlis, T. L. (Eds.), *Geology of a Transpressional Orogen Developed During Ridge-Trench Interaction Along the North Pacific Margin*, *Geological Society of America Special Paper* (Vol 371, pp. 327-353). Boulder: Geological Society of America.

Gutscher, M., Spakman, W., Bijwaard, H., & Engdahl, E. R. (2000). Geodynamics of flat subduction: Seismicity and tomographic constraints from the Andean margin. *Tectonics, 19(5)*, 814-833. doi:10.1029/1999TC001152

Haeussler, P. J., & Clark, K. P. (2000). *Geologic Map of the Wildcat Lake 7.5' Quadrangle, Kitsap and Mason Counties Washington* (Open-File Report 00-356). Reston, VA: U.S. Geological Survey.

Hagstrum, J., Booth, D., Troost, K., & Blakely, R. (2002). Magnetostratigraphy, paleomagnetic correlation, and deformation of Pleistocene deposits in the south central Puget Lowland, Washington. *Journal of Geophysical Research, 107(B4)*. doi:10.1029/2001JB000557

Heiskanen, W. A., & Vening-Meinesz, F. A. (1958). *The Earth and its gravity field*. New York: McGraw-Hill Book Company, Inc.

Hirsch, D. M., & Babcock, R. S. (2009). Spatially heterogeneous burial and high-P/T metamorphism in the Crescent Formation, Olympic Peninsula, Washington. *American Mineralogist, 94(8-9)*, 1103-1110. doi:10.2138/am.2009.3187

Hyndman, R. (1995). The Lithoprobe corridor across the Vancouver Island continental margin: The structural and tectonic consequences of subduction. *Canadian Journal of Earth Sciences, 32(10)*, 1777-1802. doi:10.1139/e95-138

Hyndman, R. D., Mazzotti, S., Weichert, D., & Rogers, G. C. (2003). Frequency of large crustal earthquakes in Puget Sound--Southern Georgia Strait predicted from geodetic and geological deformation rates. *Journal of Geophysical Research, 108(B1)*, 2033. doi:10.1029/2001JB001710

International Union of Geodesy and Geophysics (1971). *Geodetic Reference System 1967* (Special Publication 3). Potsdam: International Union of Geodesy and Geophysics.

Jachens, R. C., & Roberts, C. R., (1981). *Documentation of a FORTRAN program, 'isocomp', for computing isostatic residual gravity* (Open-File Report 81-574). Reston, VA: U.S. Geological Survey.

Johnson, S. (1984). Evidence for a margin-truncating transcurrent fault (pre-late Eocene) in western Washington. *Geology, 12(9)*, 538-541. doi:10.1130/0091-7613(1984)122.0.CO;2

Johnson, S., Potter, C., & Armentrout, J. (1994). Origin and evolution of the Seattle fault and Seattle basin, Washington. *Geology, 22(1)*, 71-74. doi:10.1130/0091-7613(1994)0222.3.CO;2

Lamb, A. P., Liberty, L. M., Blakely, R. J., Pratt, T. L., Sherrod, B. L., & van Wijk, K. (2012). Western limits of the Seattle fault zone and its interaction with the Olympic Peninsula, Washington. *Geosphere, 8(4)*, 915-930. doi:10.1130/GES00780.1

MacDonald, J. H., Jr., Dragovich, J. D., Littke, H. A., Anderson, M., & DuFrane, S. A. (2013). The volcanic rocks of Mount Persis: An Eocene continental arc that contains adakitic magmas. *Geological Society of America Abstracts with Programs, 45(7)*, 392.

Mace, C. G., & Keranen, K. M. (2012). Oblique fault systems crossing the Seattle Basin: Geophysical evidence for additional shallow fault systems in the central Puget Lowland. *Journal of Geophysical Research, 117*, B03105. doi:10.1029/2011JB008722

Magill, J. R., Wells, R. E., Simpson, R. W., & Cox, A. V. (1982). Post-12 m.y. rotation of southwest Washington. *Journal of Geophysical Research, 87*, 3761-3776.

Marshak, S. (2004). Salients, recesses, arcs, oroclines, and syntaxes -- a review of ideas concerning the formation of map-view curves in fold-thrust belts. In McClay, K. R. (Ed.), *Thrust Tectonics and Hydrocarbon Systems, AAPG Memoir* (Vol. 82, pp. 131-156). Tusla: American Association of Petroleum Geologists.

Massey, N. (1986). Metchosin igneous complex, southern Vancouver Island - Ophiolite stratigraphy developed in an emergent island setting. *Geology, 14(7)*, 602-605. doi:10.1130/0091-7613(1986)142.0.CO;2

McCaffrey, R., King, R. W., Payne, S. J., & Lancaster, M. (2013). Active tectonics of northwestern U.S. inferred from GPS-derived surface velocities. *Journal of Geophysical Research, 118(2)*, 709-723. doi:10.1029/2012JB009473

McCaffrey, R., Qamar, A. I., King, R. W., Wells, R., Khazaradze, G., Williams, C. A., Stevens, C. W., Vollick, J. J., & Zwick, P. C. (2007). Fault locking, block rotation and crustal deformation in the Pacific Northwest. *Geophysical Journal International, 169*, 1315-1340.

McCrory, P. A., & Wilson, D. S. (2013). A kinematic model for the formation of the Siletz-Crescent forearc terrane by capture of coherent fragments of the Farallon and Resurrection plates. *Tectonics, 32(3)*, 718-736. doi:10.1002/tect.20045

Merrill, R., Bostock, M. G., Peacock, S. M., Calvert, A. J., & Christensen, N. I. (2020). A double difference tomography study of the Washington forearc: Does Siletzia control crustal seismicity? *Journal of Geophysical Research: Solid Earth, 125*. doi:10.1029/2020JB019750

Molnar, P., & Tapponnier, P. (1975). Cenozoic tectonics of Asia: Effects of a continental collision. *Science, 189(4201)*, 419-426.

Morelli, C. (Ed.). (1974). *The International Gravity Standardization Net, 1971* (Special Publication 4). Potsdam: International Union of Geodesy and Geophysics.

Muller, J. (1980). Chemistry and Origin of the Eocene Metchosin Volcanics, Vancouver island, British-Columbia. *Canadian Journal of Earth Sciences, 17(2)*, 199-209. doi:10.1139/e80-016

Nelson, A., Johnson, S., Kelsey, H., Wells, R., Sherrod, B., Pezzopane, S., Bradley, L., Koehler, R., & Bucknam, R. (2003). Late Holocene earthquakes on the Toe Jam Hill fault, Seattle fault zone, Bainbridge Island, Washington. *Geological Society of America Bulletin, 115(11)*, 1388-1403. doi:10.1130/B25262.1

Parsons, T., Trehu, A., Luetgert, J., Miller, K., Kilbride, F., Wells, R., Fisher, M., Flueh, E., ten Brink, U., & Christensen, N. (1998). A new view into the Cascadia subduction zone and volcanic arc: Implications for earthquake hazards along the Washington margin. *Geology, 26(3)*, 199-202. doi:10.1130/0091-7613(1998)0262.3.CO;2

Parsons, T., Wells, R., Fisher, M., Flueh, E., & ten Brink, U. (1999). Three-dimensional velocity structure of Siletzia and other accreted terranes in the Cascadia forearc of Washington. *Journal of Geophysical Research, 104(B8)*, 18015-18039. doi:10.1029/1999JB900106

Petterson, M. G., Neal, C. R., Mahoney, J. J., Kroenke, L. W., Saunders, A. D., Babbs, T. L., Duncan, R. A., Tolia, D., & McGrail, B. (1997). Structure and deformation of north and central Malaita, Solomon Islands: Tectonic implications for the Ontong Java Plateau-Solomon arc collision, and for the fate of oceanic plateaus. *Tectonophysics, 283(1-4)*, 1-33.

Phillips, J. D., Hansen, R. O., & Blakely, R. J. (2007). The use of curvature in potential-field interpretation. *Exploration Geophysics, 38*, 111–119. doi:10.1071/EG07014

Plouff, D. (1977). *Preliminary documentation for a FORTRAN program to compute gravity terrain corrections based on topography digitized on a geographic grid* (Open-File Report 77-535). Reston, VA: U.S. Geological Survey.

Plouff, D. (2000). *Field estimates of gravity terrain corrections and Y2K-compatible method to convert from gravity readings with multiple base stations to tide-and long-term drift-corrected observation*s (Open-File Report OF-00-140). Reston, VA: U.S. Geological Survey.

Polenz, M., Hladky, F. R., Anderson, M. L., Tepper, J. H., Horst, A. E., Miggins, D. P., & Legoretta-Paulin, G. (2021). *Geologic map of the Tenalquot Prairie and northern two-thirds of the Vail 7.5-minute quadrangles, Thurston and Pierce Counties, Washington* (Map 2021-02, 47 p., 1 sheet, scale 1:24,000). Olympia: Washington Geological Survey.

Pratt, T. L., Brocher, T. M., Weaver, C. S., Creager, K. C., Snelson, C. M., Crosson, R. S., Miller, K. C., & Trehu, A. M. (2003). Amplification of seismic waves by the Seattle basin, Washington state. *Bulletin of the Seismological Society of America, 93(2)*, 533-545. doi:10.1785/0120010292

Pratt, T. L., Johnson, S. Y., Potter, C. J., Stephenson, W. J., & Finn, C. A. (1997). Seismic reflection images beneath Puget Sound, western Washington State: The Puget Lowland thrust sheet hypothesis. *Journal of Geophysical Research, 102(B12)*, 27469-27489. doi:10.1029/97JB01830

Ramachandran, K., Hyndman, R. D., & Brocher, T. M. (2006). Regional P wave velocity structure of the Northern Cascadia Subduction Zone. *Journal of Geophysical Research, 111(B12)*, B12301. doi:10.1029/2005JB004108

Reiter, K., Kukowski, N., & Ratschbacher, L. (2011). The interaction of two indenters in analogue experiments and implications for curved fold-and-thrust belts. *Earth and Planetary Science Letters, 302(1-2)*, 132-146. doi:10.1016/j.epsl.2010.12.002

Saltus, R. W., & Blakely, R. J. (2011). Unique geologic insights from 'non-unique' gravity and magnetic interpretation. *GSA Today, 21(12)*, 4-11. doi:10.1130/G136A.1

Schmandt, B., & Humphreys, E. (2011). Seismically imaged relict slab from the 55 Ma Siletzia accretion to the northwest United States. *Geology, 39(2)*, 175-178. doi:10.1130/G31558.1

Sherrod, B. L., Blakely, R. J., Weaver, C. S., Kelsey, H. M., Barnett, E., Liberty, L., Meagher, K. L., & Pape, K. (2008). Finding concealed active faults: Extending the southern whidbey Island fault across the Puget Lowland, Washington. *Journal of Geophysical Research, 113(B5)*, B05313. doi:10.1029/2007JB005060

Simpson, R., & Cox, A. (1977). Paleomagnetic evidence for tectonic rotation of Oregon Coast Range. *Geology, 5(10)*, 585-589. doi:10.1130/0091-7613(1977)52.0.CO;2

Snavely, P., MacLeod, N., & Wagner, H. (1968). Tholeiitic and alkalic basalts of the Eocene Siletz River volcanics, Oregon Coast Range. *American Journal of Science, 266*, 454-481.

Snavely, P., Wells, R., & Minasian, D. (1993). *The Cenozoic geology of the Oregon and Washington coast range* (Open-File Report 93-18). Reston, VA: U.S. Geological Survey.

Snelson, C. M. (2001). *Investigating crustal structure in western Washington and in the Rocky Mountains: Implications for seismic hazards and crustal growth* (Doctoral dissertation). El Paso, Texas: University of Texas at El Paso.

Snelson, C. M., Brocher, T. M., Miller, K. C., Pratt, T. L., & Trehu, A. M. (2007). Seismic amplification within the Seattle basin, Washington state: Insights from SHIPS seismic tomography experiments. *Bulletin of the Seismological Society of America, 97(5)*, 1432-1448. doi:10.1785/0120050204

Squires, R. L., Goedert, J. L., & Kaler, K. L. (1992). *Paleontology and stratigraphy of Eocene rocks at Pulali Point, Jefferson County, eastern Olympic Peninsula, Washington* (Report of Investigations 31, 27 p.). Olympia, WA: Washington State Department of Natural Resources.

Steely, A., Anderson, M., von Dassow, W., Reedy, T., Lau, T., Horst, A., Amaral, C., Cakir, R., West, T., Stanton, K., Linneman, C., Lockett, A., Duckworth, C., Woodring, D., Tepper, J., & Staisch, L. (2021). *Geologic and Geophysical Assessment of Tectonic Uplift and Fault Activity in the Doty and Willapa Hills, Southwest Washington: Final Report to the Department of Ecology*. Olympia, WA: Washington Geological Survey.

Swick, C. A. (1942). *Pendulum gravity measurements and isostatic reductions* (Special Publication 232). U.S. Coast and Geodetic Survey.

Tabor, R. W., & Cady, W. M. (1978a). *Geologic Map of the Olympic Peninsula* (Map I-994, scale 1:125,000). Reston: U.S. Geological Survey.

Tabor, R. W., & Cady, W. M. (1978b). *The structure of the Olympic Mountains, Washington: Analysis of a subduction zone* (Professional Paper 1033). Reston, VA: U. S. Geological Survey.

Tabor, R. W., Haugerud, R. A., Haeussler, P. J., & Clark, K. P. (2011). *Lidar-revised geologic map of the Wildcat Lake 7.5' quadrangle, Kitsap and Mason Counties, Washington* (Scientific Investigations Map 3187, 12 p., scale 1:24,000). Reston: U.S. Geological Survey. Retreived from https://pubs.usgs.gov/sim/3187/

Telford, W. M., Geldart, L. O., & Sheriff, R. E. (1990). *Applied Geophysics*. New York: Cambridge University Press.

ten Brink, U., Molzer, P., Fisher, M., Blakely, R., Bucknam, R., Parsons, T., Crosson, R., & Creager K. (2002). Subsurface geometry and evolution of the Seattle fault zone and the Seattle basin, Washington. *Bulletin of the Seismological Society of America, 92(5)*, 1737-1753.

Timpa, S., Gillis, K., & Canil, D. (2005). Accretion-related metamorphism of the Metchosin Igneous Complex, southern Vancouver Island, British Columbia. *Canadian Journal of Earth Sciences, 42(8)*, 1467-1479. doi:10.1139/E05-043

Trehu, A., Asudeh, I., Brocher, T., Luetgert, J., Mooney, W., Nabelek, J., & Nakamura, Y. (1994). Crustal architecture of the Cascadia fore-arc. *Science, 266(5183)*, 237-243. doi:10.1126/science.266.5183.237

U.S. Geological Survey (2006): Quaternary fault and fold database for the United States. Retreived from https://earthquakes.usgs.gov/hazards/qfaults

U.S. Geological Survey (1996). *Aeromagnetic map of the Roseburg area on parts of the Roseburg, Coos Bay, Medford, and Cape Blanco 1° by 2° quadrangles, Oregon* (Open-File Report 96-695, 2 sheets, scale 1:100,000). Reston, VA: U.S. Geological Survey.

Van Wagoner, T., Crosson, R., Creager, K., Medema, G., Preston, L., Symons, N., & Brocher, T. (2002). Crustal structure and relocated earthquakes in the Puget Lowland, Washington, from high-resolution seismic tomography. *Journal of Geophysical Research, 107(B12)*, 2381. doi:10.1029/2001JB000710

Walsh, T. J. (1984). *Geology and coal resources of central King County, Washington* (Open-File Report 84-3). Olympia, WA: Washington State Department of Natural Resources.

Walsh, T. J., Korosec, M. A., Phillips, W. M., Logan, R. L., & Schasse, H. W. (1987). *Geologic map of Washington - Southwest quadrant* (Map GM-34, 35 p., 2 sheets, scale 1:250,000). Olympia: Washington State Division of Geology and Earth Resources.

Warnock, A., Burmester, R., & Engebretson, D. (1993). Paleomagnetism and tectonics of the Crescent formation, northern Olympic Mountains, Washington. *Journal of Geophysical Research, 98(B7)*, 11729-11741. doi:10.1029/93JB00709

Wells, R., Burkry, D., Friedman, R., Pyle, D., Duncan, R., Haeussler, P., & Wooden, J. (2014). Geologic history of Siletzia, a large igneous province in the Oregon and Washington Coast Range - Correlation to the geomagnetic polarity timescale and implications for a long-lived Yellowstone hotspot. *Geosphere, 10(4)*, 692-719. doi:10.1130/GES01018.1

Wells, R. E., & Coe, R. S. (1985). Paleomagnetism and geology of Eocene volcanic-rocks of southwest Washington, implications for mechanisms of tectonic rotation. *Journal of Geophysical Research, 90(NB2)*, 1925-1947. doi:10.1029/JB090iB02p01925

Wells, R. E., Engebretson, D. C., Snavely, P. D., & Coe, R. S. (1984). Cenozoic plate motions and the volcano tectonic evolution of western Oregon and Washington. *Tectonics, 3(2)*, 275-294. doi:10.1029/TC003i002p00275

Wells, R. E., & Heller, P. L. (1988). The relative contribution of accretion, shear, and extension to Cenozoic tectonic rotation in the Pacific Northwest. *Geological Society of America Bulletin, 100(3)*, 325-338. doi:10.1130/0016-7606(1988)1002.3.CO;2

Wells, R. E., Jayko, A. S., Niem, A. R., Black, G., Wiley, T., Baldwin, E., Molenaar, K. M., Wheeler, K. L., DuRoss, C. B., & Givler, R. W. (2000). *Geologic map and database of the*

Roseburg 30 x 60' quadrangle, Douglas and Coos Counties, Oregon (Open-File Report 00-376). Reston, VA: U.S. Geological Survey.

Wells, R. E., & McCaffrey, R. (2013). Steady rotation of the Cascade arc. *Geology, 41(9)*, 1027-1030. doi:10.1130/G34514.1

Wells, R. E., Weaver, C. S., & Blakely, R. J. (1998). Fore-arc migration in Cascadia and its neotectonic significance. *Geology, 26(8)*, 759-762. doi:10.1130/0091-7613(1998)0262.3.CO;2

Wirth, E. A., Vidale, J. E., Frankel, A. D., Pratt, T. L., Marafi, N. A., Thompson, M., & Stephenson, W. J. (2019). Source-dependent amplification of earthquake ground motions in deep sedimentary basins. *Geophysical Research Letters, 46*, 6443-6450. doi:10.1029/2019GL082474